IAOS

International Association for Obsidian Studies

Bulletin

Number 63   **Special Issue 2020**

CONTENTS

NEWS AND INFORMATION

NEWS AND NOTES

Have news or announcements to share? Send them to IAOS.Editor@gmail.com for the next issue of the *IAOS Bulletin.*

CONSIDER PUBLISHING IN THE IAOS *BULLETIN*

The *Bulletin* is a twice-yearly publication that reaches a wide audience in the obsidian community. Please review your research notes and consider submitting an article, research update, news, or lab report for publication in the *IAOS Bulletin*. Articles and inquiries can be sent to IAOS.Editor@gmail.com Thank you for your help and support!

IAOS MEETING ONLINE FOR 2020

Due to the current COVID-19 pandemic, the SAA has canceled its annual conference in Austin, Texas, for 2020. As a result, the in-person IAOS meeting is also canceled. However, we are exploring options for a virtual IAOS meeting instead. Please watch your email for an announcement. We apologize for any hassle. Please stay healthy!

If have any questions or have items for the meeting agenda, please send them to Kyle Freund at kylepfreund@gmail.com.

ARCHAEOLOGICAL AGE COMPUTATION BASED ON OBSIDIAN HYDRATION: A SUMMARY AND CURRENT STATE OF THE ART

Alexander K. Rogers[a] and Christopher M. Stevenson[b]

[a] Maturango Museum, Ridgecrest, California, USA
[b] Virginia Commonwealth University, Richmond, Virginia, USA

Abstract

Obsidian hydration dating (OHD) is a method of computing archaeological ages based on measuring water absorption by obsidian artifacts, and is widely used in the desert west. The field has seen significant advances over the past decade, many papers having been published describing advances in the field, but to date they have not been pulled together to provide a coherent picture. This paper aims to do just that, providing a single resource for the OHD analyst. The paper describes obsidian mineralogy as it affects OHD; the effects of intrinsic water content on hydration; the mathematical form of the hydration law; the mathematics of diffusion theory; the mathematical techniques for controlling for temperature, humidity, and water content; methods for computing hydration rates, with mathematical details; and a recommended method for conducting on OHD analysis. A table of hydration rates for the south-eastern California and southern Nevada region is included. Appendices include computer codes in MatLab for OHD analysis, plus a useful workbook in MS Excel. The paper addresses OHD as currently practiced in the western United States, based on optical microscopy, and does not describe newer, experimental methods such as Secondary Ion Mass Spectrometry or infrared spectroscopy.

Introduction

Obsidian hydration dating (OHD) is a method of computing an archaeological age based on measuring the depth of diffused water in the near surface region of obsidian artifacts. Although currently less accurate than radiocarbon dating, it is also less expensive and hence larger data sets are feasible. Unlike dating by projectile point typology, OHD can be used on debitage as well, and it is the only chronometric method which can directly date obsidian artifacts. It is often the only option for chronometric assessments of sparse desert sites, where radiocarbon or dendrochronology specimens are typically lacking. Its ability to determine ages for non-diagnostic artifacts makes it useful in studies of trade and exchange, by correlating obsidian compositional data from a number of sites. Unlike radiocarbon or dendrochronology, obsidian hydration is primarily controlled by post-depositional processes of temperature and humidity, so great care is needed in controlling for environmental effects.

Obsidian hydration dating as a discipline dates from the original paper of Friedman and Smith (1960). They correctly identified the physical process involved and the mathematical form of the hydration law, and other fundamental properties of hydration. Subsequently, other advances were made, primarily by researchers in glass science and geochemistry, although, with few exceptions, no advances were made by archaeologists. The field of archaeology has gone through periods of great optimism (e.g., Friedman and Long 1976) and of complete disillusionment (e.g., Ridings 1996; Anovitz et al. 1999). In recent years the field of OHD has benefited greatly from the rigorous application of physics, geochemistry, and glass science, so that the basic physics and mathematical models are now understood, and are the basis for the present treatment.

The OHD method described here is based on usual archaeological practice applied in the western United States. The obsidian specimens are grouped by geochemical source, and a

hydration rate is ascribed to the source. The hydration rate is not adjusted for the intrinsic water content of the individual specimen. Hydration measurements are made by optical microscopy, and temperature and humidity corrections are made by calculation from meteorological records or on-site temperature measurements collected for the annual cycle. Both age and age standard deviation are computed by the model.

Analytical methods which are not general archaeological practice at present are not addressed: Secondary Ion Mass Spectrometry (Anovitz et al. [1999, 2004]; Liritzis and Laskaris [2012 and references therein]; Riciputi et al [2002]); Fourier Transform Infrared spectroscopy (Newman et al. 1986), or Infrared Photo-Acoustic Spectroscopy (Stevenson and Novak 2011).

It is assumed for this discussion that the reader is familiar with the need and technology for geochemical sourcing of obsidian specimens, and with the technique for optical measurement of hydration, so the discussion starts with obsidian hydration rims measured by a laboratory on specimens from a known obsidian geochemical source.

To begin, our discussion of the mineralogy of obsidian is described as it affects OHD, and the mechanics of the hydration process are summarized. The intrinsic, or structural, water content on hydration rate is also discussed insofar as it affects hydration rate. This is followed by an overview of the mathematical theory of diffusion to provide a basis for the subsequent discussion of temperature correction and effective hydration temperature (EHT). Computation of EHT requires temperature parameters for the archaeological site, so a method for deriving the parameters using regional temperature scaling is given; the example is for the California desert, but the user can extend the method to other areas of the world as needed. Two techniques are described for computing EHT and the resulting adjustments to the hydration rims.

Age analysis by obsidian hydration requires knowledge of the hydration rate of the obsidian, so seven methods for computing hydration rates are described, with mathematical details. Rates are tabulated for twenty-six obsidian sources likely to be encountered in the eastern California desert area. Finally, the age archaeological analysis process itself is described, including calculation of age accuracy. Computer code in MatLab for age computation is provided, along with a description of a workbook in MS Excel for chronometric analyses. The references cited are not exhaustive but will provide useful background for those interested.

Obsidian Mineralogy

Obsidian is an alumino-silicate, or rhyolitic, glass, formed by rapid cooling of magma. Like any other glass, obsidian is not a crystal, and thus it lacks the lattice structure typical of crystals at the atomic level, but it does possess a matrix-like structure exhibiting some degree of short-range spatial order (Doremus 1994:27, Fig. 2; 2002: 59-73). Obsidian is typically about 75% silica (SiO_2) and about 20% alumina (Al_2O_3) by weight, the remainder being matrix modifiers (mostly alkaline oxides) and trace elements (mostly rare-earth elements), some of which are source-specific (Doremus 2002: 109, Table 8.1; Hughes 1988; Stevenson et al. 1998; Zhang et al. 1997). The trace elements provide the means for geochemical provenance studies. The anhydrous composition (chemical composition independent of water) of obsidian from a wide variety of sources has been shown to be remarkably consistent, within a few tenths of a weight percent (Zhang et al. 1997). The minute interstices within the glass matrix, on the order of 0.1 - 0.2 nanometers in diameter, are where water penetration takes place.

All obsidian also contains small amounts of natural water, known as intrinsic water or structural water, resulting from the incomplete degassing of the lava during its ascent from the
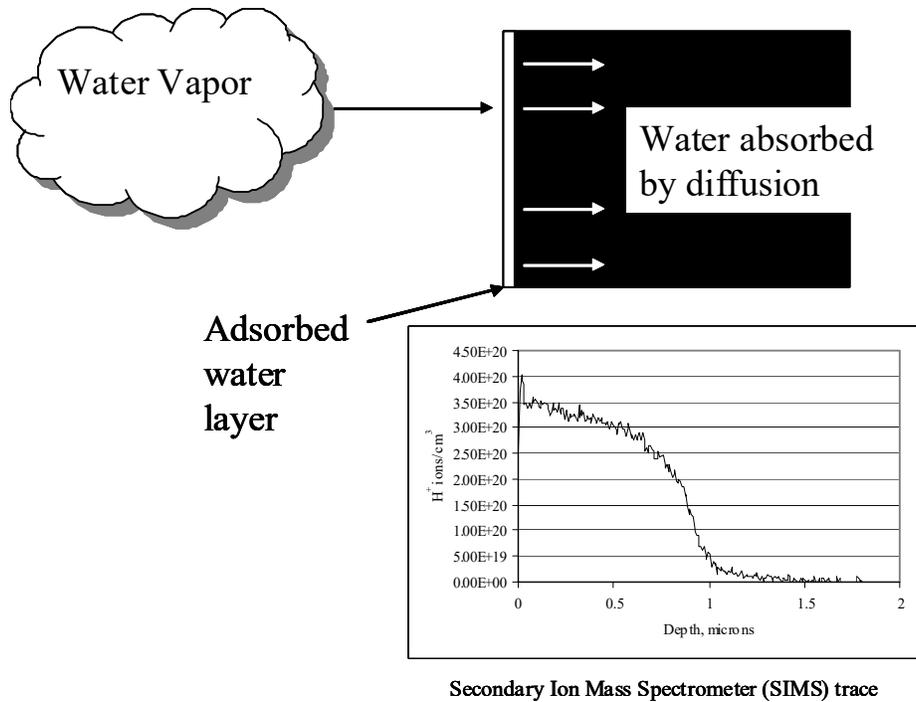
Figure 1. Schematic view of obsidian hydration. Water molecules in the atmosphere are adsorbed on the surface, and diffuse into the glass. The plot shows hydrogen ion concentration (a proxy for water) as a function of depth in the glass (SIMS trace courtesy of C. M. Stevenson). As time progresses, the curve shifts to the right.

magma chamber; the amount is generally <2% by weight in natural obsidian, although cases of somewhat higher concentration are occasionally encountered (Stevenson et al. 2018). Its effects are discussed below.

The Hydration Process

"Obsidian hydration", in its most basic aspect, simply describes the process by which water is absorbed by obsidian, and involves both physical and chemical changes in the glass (Doremus 2002; Anovitz et al. 2008). Five steps may be distinguished in the process (Figure 1).

1. When a fresh surface of obsidian is exposed to air, water molecules adsorb on the surface. Adsorption is a chemical bonding process, not simply condensation.

2. Some of the adsorbed water molecules, plus other water molecules impinging directly from the atmosphere, are absorbed into the glass and diffuse into the interstices in the glass matrix. The absorption process occurs when a water molecule has sufficient energy to stretch the glass matrix and enter one of the interstices.

3. Some of the diffusing H_2O molecules react with the silica or alumina in the glass, forming hydroxyl (OH) and causing an increase in volume and openness of the hydrated region. Since the hydrated region is expanded and the non-hydrated region is not, a stress region exists between the two. The stress region is visible under a polarizing microscope due to stress birefringence.

4. As time passes, the region of increased water concentration progresses into the glass, its rate of progress being a function of the initial openness of the glass, temperature, and the

dynamics of the process itself. Openness of the glass, in turn, is a function of intrinsic water content.

5. When the hydrated layer becomes thick enough, typically greater than 20 microns, the accumulated stresses cause the layer to spall off as perlite.

Three general classes of methods have been proposed for measuring the hydrated zone: (1) measurement of water mass uptake or loss vs. time (Ebert et al. 1991; Stevenson and Novak 2011); (2) direct measurement of water profiles vs. depth using SIMS (Anovitz et al. 1999, 2004, 2008; Riciputi et al. 2002; Stevenson et al. 2004); and (3) observation of the leading edge of the stress zone by optical microscopy (many papers, e.g., Friedman and Smith 1960; Friedman and Long 1976; Stevenson et al. 1989). The classical field of OHD is based on the third of these methods, and forms the basis of the present analysis.

In practice, hydration is measured by cutting a thin slice from the margin of an artifact with a diamond saw, mounting it on a microscope slide, polishing it to transparency, and observing it under a polarized light microscope (Michels and Bebrich 1972) (Figure 2). The thickness of the hydrated layer (the "rim" or "rind") is on the order of microns, so typically an optical magnification of 400X or more is used.

Laboratory data (Rogers and Duke 2011; Stevenson and Scheetz 1989; Stevenson et al. 1998) indicate that the position of this stress zone, or hydration front, progresses into the obsidian proportional to t^n, where n is 0.5 within limits of experimental error. Thus the hydration model employed is

$$r^2 = kt \qquad\qquad (1)$$

where t is age in calendar years, r is rim thickness in microns, and k is the hydration rate (Rogers 2007a, 2012). Although other equations have been proposed (e.g., Basgall 1991; Pearson 1994), equation (1) is the only form with both theoretical (Ebert et al. 1991; Doremus 2002) and laboratory (Doremus 1994; Stevenson et al. 1998, 2000) support.

Obsidian Composition and Hydration Rate

Obsidian anhydrous chemistry has traditionally been regarded as having a major influence on hydration rate (see attempts to determine a chemical index to hydration, e.g., in Friedman and Long 1976 or Stevenson and Scheetz 1989). In archaeological analyses, anhydrous chemistry is controlled by grouping and analyzing the obsidian by geochemical source, based on trace element composition as
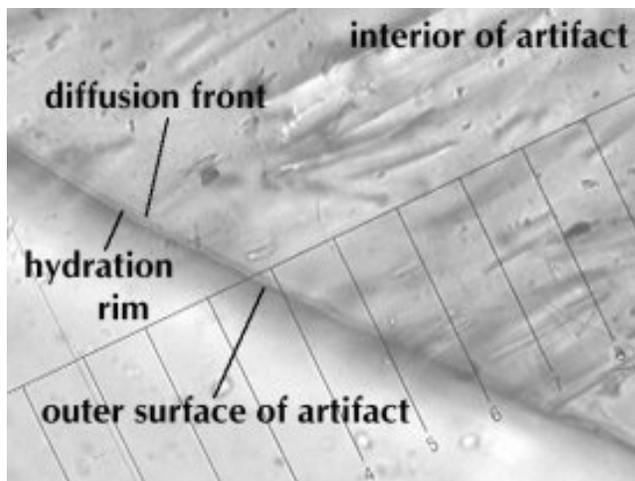
Figure 2. Cross-section of hydration rim measurement, approx. 400X. Photo courtesy of Jennifer Thatcher, Willamette Analytics LLC.
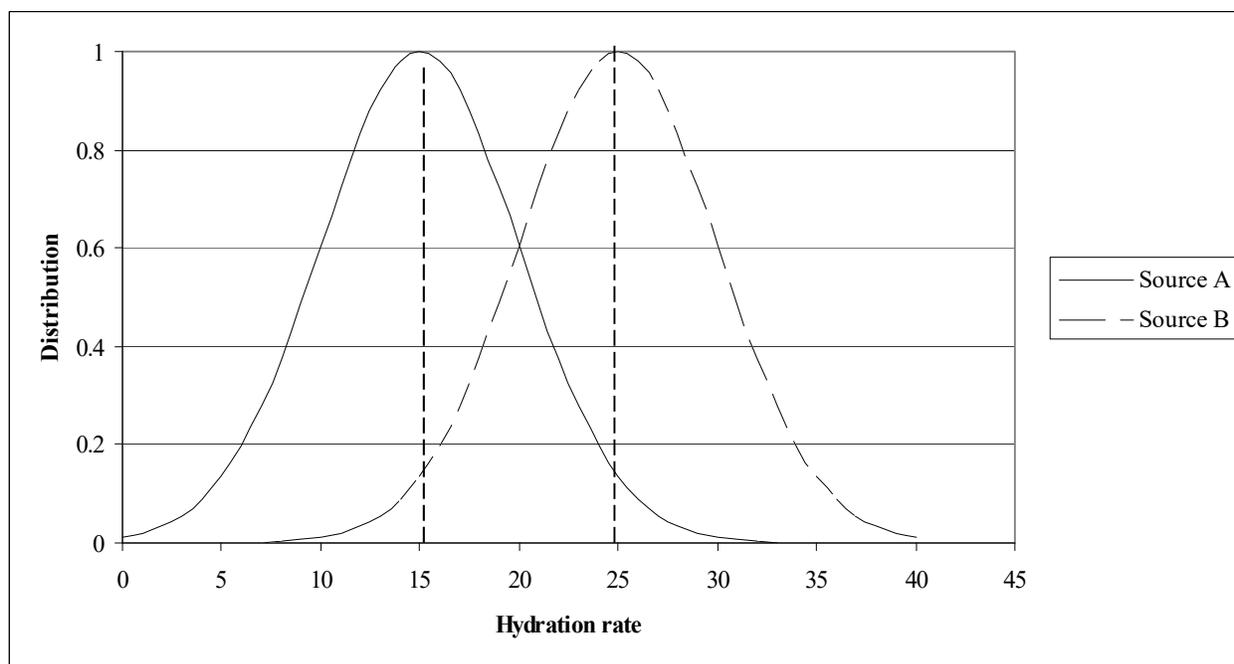
Figure 3. Hydration rate distributions for two geochemical sources. Spread is caused by intra-source variations in intrinsic water content. Geochemical sourcing controls for central tendency (dashed lines), while spread contributes of uncertainty in computed age.

determined by X-ray fluorescence (XRF) or neutron activation analysis (NAA). However, Stevenson et al. (1998, 2000) found no consistent influence of anhydrous chemistry on hydration rate. Zhang and Behrens (2000) and Behrens and Nowak (1997) found the effect of anhydrous chemistry to be negligibly small, although Karsten et al. (1982) reported that Ca^{2+} concentration may influence hydration rate to a very slight extent. It now appears that anhydrous chemistry has a negligible effect on hydration rate and attempts to predict hydration rate from anhydrous composition are unlikely to succeed.

Intrinsic water, on the other hand, has a profound effect on hydration rate since it impacts the openness of the glass structure (Behrens and Nowak 1997; Delaney and Karsten 1981; Karsten et al. 1982; Lapham et al. 1984; Rogers 2015; Stevenson et al. 1998, 2000; Zhang et al. 1991; Zhang and Behrens 2000). Four methods are currently used for measuring intrinsic water in obsidian: micro-densitometry (Ambrose and Stevenson 2004;

Stevenson et al. 2018); mass loss when obsidian powder is heated (Newman et al. 1986; Steffen 2005); mid-infrared transmission spectroscopy (Newman et al. 1986); and infrared photo-acoustic spectrometry (Stevenson and Novak 2011). However, all these techniques, except for density determination, are costly, and as currently practiced, are destructive to the artifact. As a result, intrinsic water measurement is not conducted for most practical archaeological investigations in the United States today.

Stevenson et al. (1993) analyzed the intrinsic water content of obsidian from the Coso Volcanic Field source in eastern California. Coso was known to have four geochemically distinct subsources (Hughes 1988), and Stevenson demonstrated that: (a) the mean intrinsic water content of the subsources varied between subsources, and (b) there was significant variation within each subsource. The variation in intrinsic water within a geochemical source or subsource leads to variations in hydration rate, which in turn

increases the uncertainty (statistical error) in computed ages (Rogers 2015). The effects of these errors have been analyzed in detail in Rogers (2008a, 2010).

From a practical standpoint, controlling for geochemical source actually functions as a proxy for controlling for intrinsic water (Stevenson et al. 2000), albeit rather poorly (Stevenson et al. 1993; Rogers 2008a). As shown in Figure 3, geochemical sourcing controls for the mean value (central tendency) of intrinsic water in the obsidian from that source; the uncontrolled intra-source variation in water content contributes to uncertainty in the age, and is reflected in the standard deviation of age.

Mathematical Theory of Hydration

Hydration of obsidian is known as a diffusion-reaction process (Doremus 2000, 2002); in physics, diffusion is a process in which mass is transported due to a concentration gradient, and always follows equation (1). The mathematical theory of hydration, which is based on the physical process of diffusion, is presented here to provide the background for subsequent discussion of effective hydration temperature. The obsidian hydration process is modeled physically as a diffusion-reaction process in a homogeneous medium in one dimension, described by the partial differential equation

$$\partial C/\partial t = \partial/\partial x \, (D\partial C/\partial x) - \partial S/\partial t, \quad (2)$$

where: C is concentration of diffusing molecular water, t is time, D is the diffusion coefficient, S is the concentration of water molecules which have reacted with the glass matrix, and x is depth into the glass.

As applied to hydration, the curve for C defines the concentration of molecular water as a function of depth and time. If the hydration rim, or observable region, is defined as a particular point on the curve of C vs. depth, then that point progresses according to the equation

$$x^2 = Dt \quad (3)$$

which is the familiar form of the obsidian hydration equation.

However, in the archaeological case D is not actually constant, since it is a strong function of temperature through the familiar Arrhenius equation for reaction kinetics,

$$D = A \exp [-E/(RT)]. \quad (4)$$

Here A is a constant with units of [length^2/time], E is the activation energy of the diffusion reaction in J/mol, R is the universal gas constant (8.314 J/mol °K), and T is absolute temperature in °K. Thus, since the temperature undergoes both annual and diurnal variation, D varies as well.

If D is a function of time only, a solution can be developed by a substitution of variables technique (see Crank 1975, pp. 104-105). The resulting hydration rim equation, analogous to equation (3), is,

$$r^2 = D_{eff} \, t, \quad (5)$$

where rim thickness r is substituted for x, and D_{eff} is the archaeological hydration rate, referred to as k in equation (1), and defined by

$$D_{eff} = (1/t) \int D(t') \, dt'. \quad (6)$$

Thus, if the value of D_{eff} is computed for a time-varying temperature, age can be estimated from equation (5). Substituting equation (4) into equation (6) allows computation of D_{eff},

$$D_{eff} = (1/t) \, A \int \exp\{E/[RT(t')]\} \, dt', \quad (7)$$

with T(t) defining the time variation of temperature. Since no closed-form solution to this integral is known, it must be solved numerically as a finite sum:

$$D_{eff} = (1/N) \sum A \exp\{E/[RT(t_i)]\}, \qquad (8)$$

with the sum being taken over the hydration time in N increments of $\Delta t = t_{i+1} - t_i$. An effective hydration temperature T_e (or EHT) can be defined by substituting D_{eff} into equation (4):

$$T_e = E/[R \ln(D_{eff}/A)]. \qquad (9)$$

If a time-varying temperature history can be modeled numerically, equation (8) can be used to compute an effective hydration rate constant, and an effective hydration temperature can then be computed by equation (9). The resulting EHT is a rigorous solution for time-varying D.

Eliminating D_{eff} between equations (8) and (9), substituting EHT for T_e, and rearranging terms, the effective hydration temperature is

$$EHT = -(E/R)/\ln\{(1/N) \sum \exp[E/RT(t_i)]\}. \qquad (10)$$

The sum in equation (10) is taken over at least one full cycle of the lowest-frequency variation (twelve months, in the archaeological case).

Equation (10) is important as the basis for computing EHT, which in turn is the basis for controlling for temperature in OHD. *Effective hydration temperature, defined by equation (10), is a single temperature which yields the same hydration results as the actual varying temperature over the same time.* Due to the mathematical form of the dependence of hydration rate on temperature (equation [4]), EHT is always higher than the mean temperature (except in the uninteresting case of a constant temperature, in which case they are the same). Further discussion is in Rogers (2007a, 2012).

Controlling for Temperature Effects

Effective Hydration Temperature Calculation:
Computing EHT by equation (10) requires a mathematical model of the temperature history for the artifact. The temperature at an archaeological site can be modeled as the sum of a mean temperature and two sinusoids; one with 24-hour period and the other with a 12-month period. The constant term is the annual average temperature, T_a. The sinusoid with a twelve-month period is the annual variation, V_a, and describes the variation of monthly average temperatures through the year. The sinusoid with a 24-hour period is the mean diurnal variation, V_d, describing the daily hot and cold cycle. A technique to determine the amplitudes T_a, V_a, and V_d for any given archaeological site is described below under temperature estimation. Temperatures have also varied over longer archaeological time scales, which can introduce an error into age estimates made based on current conditions. A technique to correct for this is also described below.

For buried artifacts, V_a and V_d must represent the temperature variations at the artifact burial depth, which are related to surface conditions by

$$V_a = V_{a0}\exp(-0.44z) \qquad (11a)$$

and

$$V_d = V_{d0}\exp(-8.5z) \qquad (11b)$$

where: V_{a0} and V_{d0} represent nominal surface conditions and z is burial depth in meters (Carslaw and Jaeger 1959:81). (Note that the similar equations in Rogers [2007a, 2012] are incorrect). Depth correction for EHT is desirable, even in the presence of site turbation, because the depth correction, on the average, gives a better age estimate (Rogers 2007b).

The time increment in the numerical integration for equation (10) is one hour, and the period of integration is one year. In a practical sense, numerical integration of equation (10) requires a mathematical software package such as MatLab or Mathematica; it can be performed by MS Excel, but, with a 1-hour

time increment, it requires a spreadsheet with 8760 lines, which is cumbersome, slow, and prone to errors. Computer code in MatLab to perform the computation is in Appendix A; it will also execute under the Gnu Octave software environment, but the user must still know how to program in MatLab.

Since MatLab is not generally available in the archaeological community, an algebraic approximation was developed. A large number of runs were made with MatLab for temperature parameters typical of archaeological sites, and a best fit equation developed. The resulting equation for EHT, which specifically accounts for average annual temperature, mean annual temperature variation, mean diurnal temperature variation, and burial depth, is

$$EHT = T_a + 0.0062*Y \qquad (12a)$$

where: T_a is annual average temperature, and the variation factor Y is defined by

$$Y = V_a^2 + V_d^2 , \qquad (12b)$$

in which V_a and V_d are as defined above (note that equation [12a] is a simplification of the corresponding equation in Rogers 2007a and 2012). All temperatures are in degrees centigrade. For typical desert conditions, equation (12a – b) agrees with the results of equation (10) to within 0.25°C, 1-sigma. Equations 12(a – b) are built into the MS Excel spreadsheet described further below.

Once EHT has been computed, either by equation (10) or equation (12a – b), the measured rim thickness r_m is multiplied by a rim correction factor (RCF) to adjust the rims to be comparable to the EHT for which the hydration rate was measured:

$$RCF=\exp\{[(E/R)/(EHT_s+273.15)-(E/R)/(EHT_r + 273.15)]/2\} \qquad (13)$$

where: E and R are defined as above, EHT_s is

the EHT computed for the specimen, and EHT_r is effective hydration temperature for which the hydration rate was computed.

Values of E/R for obsidians range from ≈ 9000°K to ≈11000°K (Friedman and Long 1976), and are a function of intrinsic water content by the equation

$$E/R = 10433 - 1023*w \qquad (14)$$

where: w is total intrinsic water in wt% (Rogers 2015). If intrinsic water content is unknown, use of E/R = 10000°K is a good approximation (Rogers 2015). In the MatLab model for EHT, temperature and hydration rate are used to compute E/R, which is then used in equation (13) to compute RCF; the MS Excel model uses a single value of E/R of 10000°K.

The EHT-adjusted rim value r_c is then

$$r_c = RCF \times r_m \qquad (15a)$$

The value r_c is then used in equation (1) to compute age. Further, the EHT-adjusted rim standard deviation is

$$\sigma_c = RCF \times \sigma_m \qquad (15b)$$

where: σ_c is the corrected standard deviation and σ_m is the standard deviation as measured by the laboratory.

Site Formation Processes:
The EHT that an obsidian artifact is exposed to is a strong function of burial depth, and, for deeply buried artifacts, can significantly affect the age computed by OHD since temperatures below the surface may be substantially cooler by several degrees. Computing age based on higher temperature surface conditions and ignoring the effects of burial depth will invariably yield an age which is too young. On the other hand, if the burial conditions have varied significantly over time, computing age based on the deepest burial depth may yield ages which are too old. An

example of the latter would be deeply buried artifacts eroding out of a dune field.

The preferred method for accounting for changes in depth is time-averaging, whose physical basis is that the overall hydration rate is the time-average of the instantaneous rate, over the temperature history of the artifact (equation [6], above). Note that this is not the same as the hydration rate for the average temperature, nor the hydration rate for the average depth. It is immaterial whether the artifact is buried and then exposed or vice versa (Duke and Rogers 2013). The principle is to compute the hydration rate at depth and on the surface, and then compute a weighted average based on what fraction of its life the artifact was buried. The technique is complex computationally and requires an application such as MatLab (Rogers and Yohe 2016). The computer code in Appendix A accounts for the length of time an artifact was buried, as well as the depth, based on a user-input value of the fraction of the artifact's life that it was buried. The algorithm computes an average value of the diffusion coefficient over time and uses this value to compute age. It includes this uncertainty in the age standard deviation.

The second, simpler, method is level averaging. It is somewhat less accurate than time-averaging, but, in view of the large standard deviations created by site formation processes, it is still a reasonable approximation. The principle is to decide on two limiting cases for depth, such as the recovery depth and the surface. Ages are computed for each depth, and a simple average computed as the best estimate of the age, which can be performed in MS Excel. In both methods, the standard deviation of computed age due to site formation is the difference of the two limiting ages divided by $\sqrt{12}$.

In a case where there are no data to suggest the time phasing of the site formation, either is adequate. However, if geoarchaeological or other contextual data are available such that timing of the phases of the burial process could be estimated, then the time-averaging method is preferable.

Temperature Parameter Estimation:

Temperature parameters can be computed from meteorological records, available at no cost from the Western Regional Climate Center (WRCC). It is important to use long-term data in these computations, and 30 years is the standard for determining climatological norms (Cole 1970). Two cases are discussed here: the

HAIWEE, CALIFORNIA (043710)

1971-2000 Monthly Climate Summary

	Jan	Feb	Mar	Apr	May	Jun	Jul	Aug	Sep	Oct	Nov	Dec	Annual
Average Max. Temperature (F)	52.7	57.7	63.6	70.6	79.7	89.7	95.7	93.9	87.0	76.1	60.4	53.3	73.6
Average Min. Temperature (F)	29.1	32.4	36.8	42.2	50.0	58.2	63.8	62.6	56.1	45.9	34.2	28.9	45.1
Average Total Precipitation (in.)	1.26	1.64	1.09	0.40	0.30	0.10	0.32	0.41	0.34	0.19	0.48	0.90	7.43

Figure 4. Western Regional Climate Center web page for Haiwee California, showing typical format. Site elevation is accessed by clicking a button labeled "Site Metadata".

	J	F	M	A	M	J	J	A	S	O	N	D
MaxF	52.70	57.70	63.60	70.60	79.70	89.70	95.70	93.90	87.00	76.10	60.40	53.30
MinF	29.10	32.40	36.80	42.20	50.00	58.20	63.80	62.60	56.10	45.90	34.20	28.90

$^{o}C = (5/9)*(^{o}F - 32)$

	J	F	M	A	M	J	J	A	S	O	N	D
MaxC	11.50	14.28	17.56	21.44	26.50	32.06	35.39	34.39	30.56	24.50	15.78	11.83
MinC	-1.61	0.22	2.67	5.67	10.00	14.56	17.67	17.00	13.39	7.72	1.22	-1.72
Mnth Ave	4.94	7.25	10.11	13.56	18.25	23.31	26.53	25.69	21.97	16.11	8.50	5.06
Diur. Rng	13.11	14.06	14.89	15.78	16.50	17.50	17.72	17.39	17.17	16.78	14.56	13.56

T_a	15.11	^{o}C	Average of MaxC and MinC
V_{a0}	21.58	^{o}C	Hottest-month mean minus coldest-month mean
V_{d0}	15.75	^{o}C	Average of diurnal range

Figure 5. Computation worksheet to compute temperature parameters for Haiwee, California.

situation in which there is a meteorological station near the archaeological site, and the situation where there is not. In each case an example is given to illustrate the process.

If there is a nearby meteorological station, data from the station can be downloaded from the WRCC website (www.wrcc.dri.edu) and used as a proxy for conditions at the site. As an example, the Rose Spring site (CA-INY-372) is within a mile of the power plant at South Haiwee Dam and at the same elevation, which provides a data set. Figure 4 shows the web page data set which can be copied and pasted into an MS Excel spreadsheet.

The temperature data are reported in °F, so the first step is to convert to °C (°C = 5*[°F - 32]/9). Next the overall average is computed, which is T_a. The average for each month is then computed, and V_a is the hottest month mean minus the coldest month mean (typically August minus January). Finally the diurnal range is computed, and its mean is V_d. Figure 5 illustrates the calculations. With T_a, V_a, and V_d known, the EHT can be computed.

Unfortunately, many archaeological sites are not co-located with meteorological stations and furthermore, there may be considerable variations in elevation, which affects temperature. In such a case, typical of much of the desert west, temperature parameters can be estimated by regional temperature scaling. The scaling principle is that desert temperature parameters are a strong function of altitude above mean sea level, and the estimates of temperature can be determined by scaling from 30-year data from large a number of meteorological stations. An example is presented from the upper Mojave Desert.

The analysis is again based on monthly temperature data from the Western Regional Climate Center. Fourteen meteorological stations were used, ranging from 940 to 11,470 ft amsl. In each case the data were downloaded from the WRCC website and parameters computed as shown for the Haiwee case above. Table 1 shows the data.

The expected form of the best-fit scaling equation is y = a + b*h, where y is the temperature parameter, a is the y-intercept, b is the slope (known meteorologically as the lapse rate), and h is altitude. The best fit equations can be computed easily with MS Excel, with results as in Table 2.

Thus, temperature parameters for any site in the upper Mojave Desert can be predicted based on site altitude. Effective hydration temperatures computed based on the model agree with those from the stations to within 0.63°C, 1-sigma.

Site	Altitude, ft	T_a, °C	V_a, °C	V_d, °C
Baker	940	21.27	25.25	17.55
Trona	1700	19.29	24.36	16.31
Daggett Airport	1930	19.72	22.56	15.63
Cantil	1960	17.88	23.08	18.30
Barstow	2140	17.71	21.58	18.20
China Lake NAF Armitage Field	2240	17.68	23.78	18.12
Inyokern	2440	17.70	21.94	18.50
Mojave	2740	17.13	21.44	14.37
Haiwee	3282	15.38	22.31	15.02
Randsburg	3570	17.03	21.47	13.62
Wildrose	4100	14.86	21.53	14.93
Bishop	4150	13.37	21.92	20.46
Mountain Pass	4700	14.39	22.06	13.60
White Mountain 2	12470	-2.51	16.94	9.48

Table 1. Temperature parameter data, upper Mojave Desert

In addition, the mean diurnal variation varies in a consistent manner through the year. The effect is small, but can be modeled as

$$V_d(m) = V_d + 2.08*\cos(6*m*\pi) \qquad (19)$$

where m is the number of the month (1 - 12) and V_d is as defined above. The effect on EHT is small, and is modeled in the MatLab code but not in the MS Excel spreadsheet.

Parameter	y-intercept, °C	Slope, °C/ft	R^2
T_a	22.71	-0.0020	0.9814
V_a	24.25	-0.0006	0.7949
V_d	18.49	-0.0007	0.5178

Table 2. Temperature scaling, upper Mojave Desert

These equations are for air temperatures. Obsidian on the surface is exposed to surface temperatures, which can be significantly higher than air temperatures in areas devoid of vegetation (Johnson et al. 2002; Rogers 2008b). However, a detailed analysis based on data from Rose Spring (CA-INY-372) has shown that meteorological air temperature gives a good estimate of surface ground temperature in situations in which even intermittent shade is present (Rogers 2008c). In regions entirely void of vegetation, temperature sensors may be needed to measure ground temperatures.

Caves and rockshelters affect the annual and diurnal variation to a significant degree because sunlight is blocked by the surrounding rock. Temperature sensor measurements performed in Ray Cave (CA-INY-444) showed that the annual variation (monthly mean for hottest month minus monthly mean for coldest month) inside the cave was about 75% of the variation outside. For archaeological calculations, V_a can be determined by a meteorological model and then multiplied by 0.75. Diurnal variation within caves has been measured to be approximately 5°C, year around (Everett-Curran et al. 1991).

Paleotemperature Effects:

The usual assumption is that the parameters which characterize the current temperature regime, whether determined by use of sensors or meteorological records, are a reasonable approximation to ancient temperatures. The assumption is generally valid for ages in the Holocene. However, multi-proxy data have been published which show significant shifts in ancient temperatures relative to the present (e.g., Bintanja et al.
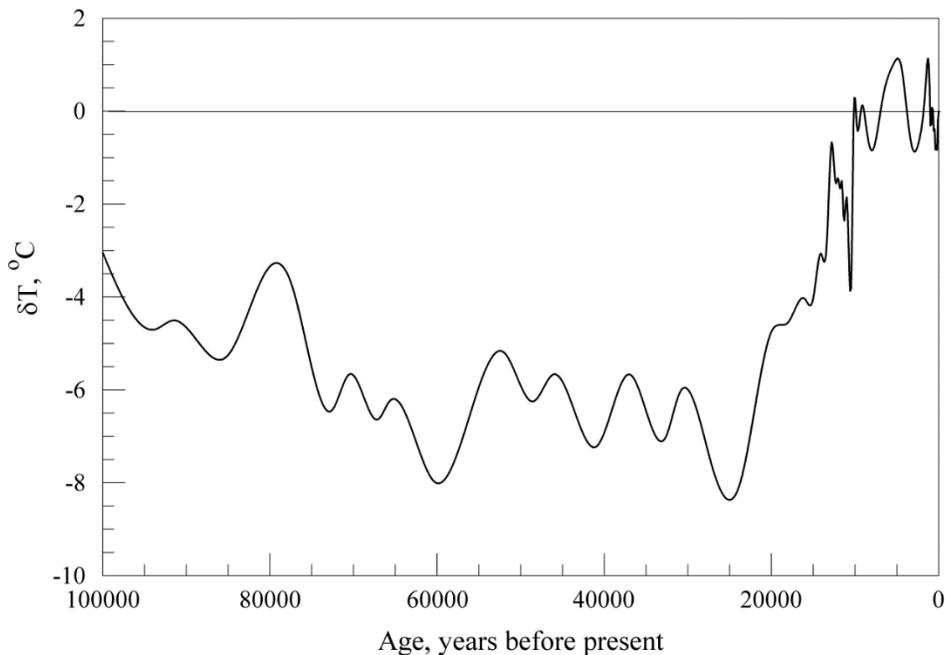
Figure 6. Changes in regional-scale mean temperatures since the middle Pleistocene, reconstructed from multi-proxy data by Stineman interpolation (Bintanja et al. 2005; West et al. 2007:17, Fig. 2.2).

2005; West et al, 2007), especially for ages before approximately 12 - 13Kya (Figure 6). Data sources include marine fossils, tree-ring data, studies of *Neotoma* nest contents, pollen records, and Greenland ice cores (Bintanja et al. 2005; West et al, 2007). For these ages the prevailing temperatures were significantly cooler than today, and ages computed assuming current conditions will be too young.

The key parameter in temperature studies of obsidian is EHT, rigorous computation of which requires all three of the temperature parameters. These can be easily determined for current conditions, but the situation is different for ancient climates. As described above, the published temperature summaries such as seen in Figure 6 are based on proxy data, and represent changes in mean annual temperatures, but similar proxy data showing how annual and diurnal temperature variation have also changed over time have not been published. However, changes in both annual mean temperature and the annual and diurnal

temperature variations are driven by the same mechanism: changes in insolation caused by changes in the earth's orbit; thus, it is likely that the annual and diurnal temperature variations have varied in proportion to variations in average annual temperature. By this model, the change in EHT over geologic time scales can be represented by the change in mean annual temperature.

Rogers (2015b) reported an analysis of the effects of paleotemperature shifts on OHD, based on temperature proxy data back to 200Kyrs, and on the assumption that any changes in EHT over time are equivalent to changes in mean temperature. The method was to compute the hydration rate for each 100-year segment, using proxy data for the annual average temperature and assuming no change in annual or diurnal variation. The analysis then assumes a date for an artifact and computes the average hydration rate since that date. It was found that the effects of paleotemperature shifts on hydration rate are negligible for ages less than about 13,000 years; for earlier ages a

correction should be applied. Details of the analysis and correction method, including spreadsheet and MatLab tools, are in Rogers (2015b).

Temperature Sensors:

Temperature sensors at a site are sometimes necessary for determining temperature parameters, but must be used with care. Today, digital sensors such as Hobo™ sensors are available at very low cost and are the preferred method for measuring temperature. Such devices incorporate both a sensor and a data logger, and can be set to sample temperatures at any desired hourly interval. Sensors should be placed at the site and left undisturbed for a year, then removed and down-loaded. The temperature parameters can be computed from the data set (Rogers 2008b).

A caveat is that temperature sensors do not represent 30-year data, so their data should be used with care. Sensor data should be compared with meteorological records to ensure that any difference is due to conditions at the site and not to an anomalous year.

Humidity Effects:

Ebert et al. (1991) reported that the hydration rate is affected by relative humidity, measured by steady-state mass gain. Friedman et al. (1994) used a similar mass gain protocol, and again reported a humidity dependence. However, Mazer et al. (1991), using optical microscopy, reported that the hydration rate was relatively unaffected by humidity, as long as humidity was under about 80%. Above that level, the hydration rate increased by a factor of approximately 1.2 between 90% and 100% relative humidity, so clearly there is an effect.

Unfortunately, humidity trends, unlike temperature trends, are highly random and are virtually impossible to model deterministically, so they can only be incorporated statistically. If humidity varies randomly between 90% and 100%, the reported factor of 1.2 in rate corresponds to a coefficient of variation of

about 6% in rate (= $0.20/\sqrt{[12]}$). This factor is included in the MatLab code in Appendix A, but was not included in the code documented in Rogers 2018. It is included in the MS Excel workbook (Appendix C).

Temperature Model Validity:

The temperature model used for computing EHT is fairly simplistic: a constant term plus two sinusoids, one of 12 month period and the other of 24 hour period, with no adjustment for annual variation in length of daylight hours. An analysis was performed to validate the model against field data, using three years of temperature data from the USGS Amargosa Desert Research Site at Beatty, Nevada; data were from Johnson et al. (2002). The approach was to compute temperature parameters from the data stream and construct a temperature model; the model was then used in equation (10) to compute EHT. In parallel, EHT was computed from equation (10) directly using the sensor data stream as the temperature model. Agreement within 1°C was obtained, and so the model is deemed adequate for archaeological use (Rogers 2008b).

Cautionary Points:

There are three phenomena which can damage an obsidian specimen and thereby affect the validity of an OHD analysis: chemical erosion, mechanical erosion, and heat. Chemical erosion has been discussed by Morgenstein et al. (1999) for the case of soda-lime glass. Using scanning electron microscopy (SEM), they found that water containing Na+ and K+ ions caused erosion of the glass surface. Although data are lacking for obsidian, it is chemically similar to soda-lime glass and such erosion is possible. It would be most likely to occur in extreme chemical conditions such as dry playas, but the phenomenon has not been reported archaeologically.

Mechanical erosion occurs primarily due to wind-blown sand in desert regions and beach

dune deposits. In severe cases, the abrasion can obliterate the surface layer of the obsidian. If an internal step-fracture can be located on the specimen, a valid rim may be identified within an internal fissure and the protected hydration layer measured. It is possible that rapidly-flowing, sediment-laden water could cause the same erosion, but it has not been reported.

Since obsidian hydration is a temperature-dependent process, OHD is affected by post-depositional heat exposure of a specimen. Sustained, intense fires, such as forest fires or camp fires in excess of 400ºC, will make the hydration rim unreadable, and in extreme cases will destroy the specimen (Steffen 2005). However, lower temperature grass fires typically have no effect. The hydration analyst will be able to detect fire effects on obsidian, since it usually causes a diffuse hydration rim. Also, obsidian, unlike crypto-crystalline silicates, cannot be heat-treated to enhance flaking. The effect of heat-treating is to cause vitrification of the material, which fuses the crystalline grains into a glass. Since obsidian is already a glass, heat-treating has no benefit. Furthermore, excessive heat will destroy the specimen (Steffen 2005).

Hydration Rate Determination Methods

The hydration rate at ambient temperature is the other key parameter needed for OHD. Hydration rates can be estimated by any of a number of methods, the most common of which are radiocarbon association, temporally-sensitive artifact association, artifact baselining, laboratory induced hydration, intrinsic water calibration, curve re-fitting, and inter-method proportionality. Each technique is described in detail below.

Radiocarbon Association:

The classic method for computing a hydration rate is by obsidian-radiocarbon association. The principle is to measure the hydration rims for a number of obsidian specimens from contexts of different time periods that are associated with radiocarbon dated organic materials. The underlying assumption of the method is that the two materials entered the archaeological record at approximately the same time. The obsidian layer thicknesses are then adjusted to a common EHT value (equations [13] and [15a], above), and a least-squares best fit computed to the calibrated radiocarbon data. A hydration rate can then be computed based on equation (1).

Obsidian specimens for inclusion in hydration rate computation should be selected with care. First, they must be geochemically analyzed, and segregated by geological source in order to control for the variation in structural water content that can impact the rate of hydration. Second, they should be from a known archaeological provenience; in particular, site elevation and specimen burial depth should be known, since both affect the EHT computation. Finally, it is wise to document carefully which specimens are used in the computation, with full and careful citation of published documents so the data are traceable.

Prior to use in rate computation, all obsidian readings from each geological source must be adjusted to a common EHT, which includes the effects of site elevation and specimen burial depth. In the California desert, 20°C is an appropriate standard EHT, while in cooler climates such as Oregon, 12°C is typically used (J. Cowan, pers. comm. 2019). Whichever value is chosen, all hydration rims must be adjusted to it, both in rate computation and in age calculation. The mathematics to make the adjustment were fully described above.

Radiocarbon specimens should also be selected with care. Dates from stationary features such as hearths are the best, since they are not normally affected by bioturbation, and obsidian specimens should be stratigraphically linked to the feature. Radiocarbon ages should always be converted to calibrated years, using one of the standard packages such as OxCal or

Calib. Since most of the obsidian work has been done closer to the year 2000 than to 1950 (the radiocarbon "present"), it is preferable to use 2000 as the present. Ages in this system are calibrated years before 2000, or cyb2k (cyb2k = calibrated age + 50).

The decision of which ages to associate with the rims is often a matter of judgment about the integrity of archaeological context and its impact on the strength of the obsidian/radiocarbon sample association. As a result, this situation is frequently the major source of uncertainty in the calculated hydration rate. In particular, it should be borne in mind the obsidian is likely to migrate vertically within a site, either by bioturbation or by human reuse of obsidian debitage, so the association with radiocarbon dated samples may be spurious. Establishing an association between obsidian and radiocarbon samples is always a matter of detailed observation and interpretation, and is the major source of uncertainty.

Rate Computation:

It is well known that the development of the hydration rim in obsidian proceeds as described by equation (1) above. Thus, the hydration rate is a slope, and can be computed by least-squares best fit methods. The physics of the situation (zero rim at zero time) dictates that the best fit line must pass through the origin.

Consider a general data set of N pairs $\{x_i, y_i\}$, in which the y_i values are assumed to include random errors and the x_i values are assumed error-free; the assumption that the independent variable is error-free is a fundamental aspect of least-squares fitting, which is met to a greater or lesser degree with real data sets (Cvetanovic et al. 1979; Meyer 1975). Assume further that a theoretical model suggests a linear relationship between the two, and that the best fit line is constrained to pass through the origin as in equation (1). The least-squares best fit method then yields a slope of

$$S = \sum w_i x_i y_i / \sum w_i x_i^2 \qquad (20)$$

(Cvetanovic et al. 1979:52, eq. 6), which minimizes the mean-square errors in y. Here the sums are taken over all N data points, and w_i is a weighting factor, typically chosen to be $1/\sigma_i^2$, where σ_i is the standard deviation of the errors in y associated with the ith data point Note that σ_i is not the difference between the ith data point and the best fit line.

In applying equation (20), it is possible to choose either time (t), rim value (r), or the square of the rim value (r^2) as the independent variable x. An obvious first choice is to use t as the independent variable and r^2 as the dependent variable, since this matches the physical process and the resulting slope yields the rate directly. However, the best fit procedure is based on the assumption that the independent variable is error free, which is clearly not the case here, since there are errors (i.e., uncertainties) in both the hydration rim value and the assumed age. Furthermore, the uncertainties in t are dominated by the association problem, so they are typically much greater than uncertainties in r. Thus, t is not a good choice for the independent variable.

Choosing between r and r^2 as independent variable depends on propagation-of-error theory (Taylor 1982). It can be shown that the error coefficient of variation (CV) for r^2 is twice that of r. Thus, choice of r as the independent variable and sqrt(t) as the dependent variable minimizes the errors associated with the rate estimate, and is the recommended approach, so the mean value of the hydration rate is

$$k = 1/S^2 \qquad (21)$$

Once S has been computed, the next step is to compute the standard deviation of the slope. The best-fit value of y_i (designated $\hat{y}_i$) is then given by

$$\hat{y}_i = S x_i \qquad (22)$$

The error between the best fit and the measured data is then

$$\delta_i = \hat{y}_i - y_i \tag{23}$$

Finally, the standard deviation of the slope value S is (Cvetanovic et al. 1979:52, eq. 6e)

$$\sigma_S = \text{sqrt}\{\sum w_i \delta_i^2/[(N-1)\sum w_i x_i^2\} \tag{24}$$

and the CV_s of the slope is σ_S/S. The CV of the rate is $CV_k = 2 \times CV_s$, and the standard deviation of the rate is then

$$\sigma_k = CV_k \times k = 2 \times CV_s \times k \tag{25}$$

Appropriate values for the weighting factors w_i must also be defined. If each data point is comprised of an average of N_i values, then $w_i = N_i$; otherwise, $w_i = 1$ is the default value unless there is an *a priori* reason to place greater weight on particular data points.

Thus, given a set of data points and a model of the physical process, the mean and standard deviation of the hydration rate can be computed. Accuracies of 5% are achievable with this method (Rogers 2010) with the association problem being the chief source of uncertainty.

Temporally-Sensitive Artifact Association:

If radiocarbon data are not available, a rate can often be computed based on temporally-sensitive artifacts, particularly projectile points. The use of temporally-sensitive artifacts is not a new approach (e.g. Pearson 1995), but the process is fraught with peril. Should the analyst use the median age for each point type, or try to determine transition points between types? Is the use of either the median or the transition points applicable for very long-lived types such as Elko? Does including long-lived point types improve or degrade the rate estimate?

The method described here addresses these issues by including a confidence-based weighting factor for each data point (Rogers and Duke 2014a). The weighting factors are not arbitrary but are based on the inverse of the known age span of the artifact type; the longer the span, the lower the confidence in the artifact's true age. The analysis assumes the hydration rim data have been corrected for effective hydration temperature (EHT) using the method described above, including the effects of site elevation, burial depth of the artifact, and site formation processes.

The mathematical method for this approach is the same as that for radiocarbon association, except that now values for the weighting factors w_i must also be defined that are appropriate for temporally-sensitive artifacts. The age assigned to a particular artifact is typically the mean or median age for the type. For example, the Rose Spring point is generally considered to have been manufactured between approximately 1600 cal BP (Yohe 1992, 1994) and 650 cal BP Justice (2002:321); by contrast, the Elko point type was exceptionally long-lived, from approximately 7800 cal BP to 1800 cal BP (Smith et al. 2013:588, Fig. 3). Thus the Rose Spring type would be assigned an age of 1125 cal BP, and the Elko 4800 cal BP.

However, the confidence associated with these ages differs, since the Rose Spring was manufactured over a span of only 950 years, while the Elko span was 6000 years; the shorter the span, the higher the confidence, so the weighting factor should be inversely related to the time span. The objective is to use a weighting factor which favors short time spans, so a simple form for the weighting factors is

$$w_i = 1/(t_b - t_e)^2 \tag{26}$$

where t_b is the beginning age for a given point type and t_e is the ending age. Strictly speaking, the denominator of equation [26] should be divided by sqrt(12), to give the standard deviation; however, any constant factor cancels out of equation [20], so the simpler form of

equation [26] gives the same slope value. Thus, the mean and standard deviation of the hydration rate can be computed by using the weighting factors from equation (10) in the best fit process described for radiocarbon association.

Hydration rates computed by this method will probably be less accurate than those developed with radiocarbon dates because of the greater age uncertainties connected with projectile point forms. In addition, artifact time spans will differ between the eastern and western Great Basin, and are subject to differences in published artifact typology. However, sometimes this is the only method available to establish chronological control over an archaeological deposit.

Artifact Baselining:

If two temporally-sensitive obsidian artifacts of the same type but different geochemical sources are recovered from the same context at a site, and the rate is known for one of the sources, the rate for the other source can be computed since the hydration rates are proportional to the square of the rim readings.

As an example we look at the Tulare Lake Wide-Stemmed points from the Witt Site (CA-KIN-62) in the San Joaquin Valley of California (Rogers 2012b). The projectile points were all of the same type, and were recovered in the same context. One set of points was sourced to Coso West Sugarloaf (WSL), the other set to Casa Diablo Sawmill Ridge (CDSR). The hydration rate for WSL is known (18.14 μ^2/1000 yrs @ 20°C, Rogers 2015a), so the hydration rate for CDSR can be computed analytically by assuming that the projectile points were manufactured at approximately the same time, irrespective of obsidian source; that they experienced similar temperature histories; and that the growth of the hydration rim is proportional to the square-root of time.

The analysis is based on equation (1):

$$r^2 = kt \qquad (1)$$

where: r is the hydration rim measurement, t is age, and k is the hydration rate. If we assume that the points are of the same age, regardless of obsidian source, that they have experienced the same temperature history, and that we know the hydration rate of one source such as WSL, then the hydration rate of any other source such as CDSR is

$$k_{CDSR} = k_{WSL} \times (r_{CDSR}/r_{WSL})^2 \qquad (27)$$

For the particular case in point, this led to a rate for CDSR of 12.70 μ^2/1000 yrs @ 20°C.

There is a major caveat to this method. In addition to the assumption of the same temperature history, it makes an implicit cultural assumption that the two obsidian sources were exploited roughly contemporaneously. In the case of the Tulare Lake Wide-Stemmed points from the Witt Site, the CDSR hydration rate yields archaeologically reasonable ages when applied to other sites and contexts, so this cultural assumption is probably valid. By contrast, when this method was applied to two obsidian sources recovered at Bonneville Estates Rockshelter in western Utah, it did not work. (Rogers and Duke 2018). Subsequent analyses showed the two sources (Brown's Bench and Topaz Mountain) had been exploited at significantly different times, which invalidated this method. (Rogers and Duke 2018) Thus, this method must be treated with caution, and resulting rates cross-checked for validity.

Laboratory Induced Hydration:

This technique takes advantage of the known temperature-dependence of the hydration process. In this method, the rate of hydration is measured at elevated temperatures, where the reaction occurs within weeks instead of millennia, and then corrected to reflect archaeological temperature. An analysis starts by combining equations (1) and (4) to yield

$$r^2/t = k_0*exp*(-E/RT) \qquad (28)$$
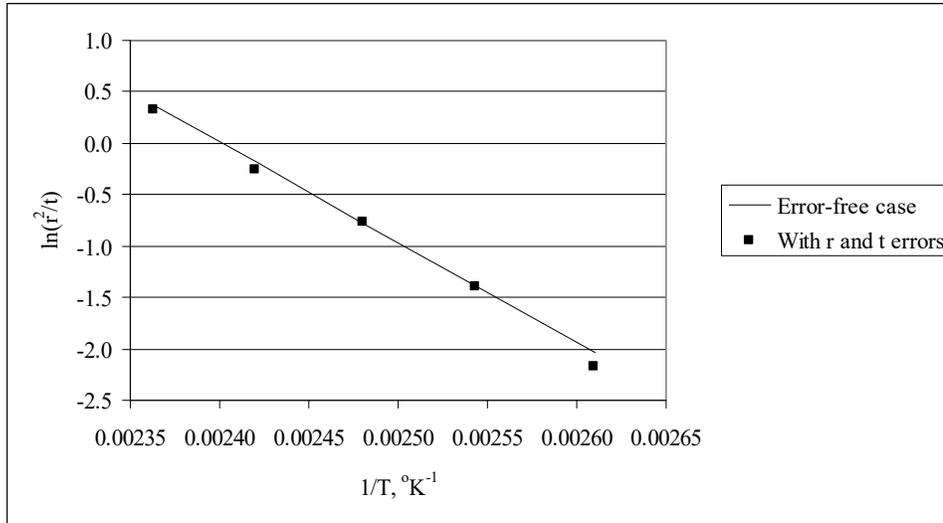
Figure 7. Illustration of a log-Arrhenius plot for laboratory induced hydration. The slope = -E/R, and the y-intercept = ln(k_0).

Taking the natural logarithm of each side gives the so-called logarithmic Arrhenius equation

$$\ln(r^2/t) = \ln(k_0) - E/RT. \tag{29}$$

If we define

$$y = \ln(r^2/t) \tag{30}$$

and

$$x = 1/T, \tag{31}$$

equation (3) becomes a linear equation of the form

$$y = I + Sx \tag{32}$$

with I = ln(k_0) and S = -E/R (Figure 7). Given data for r, t, and T for three or more points, equation (6) can be solved as a weighted least-squares linear best-fit not constrained to pass through the origin (Cvetanovic et al. 1979; Meyer 1975); S is the slope and I is the y-intercept given by

$$S = \{\sum w_i \sum w_i x_i y_i - \sum w_i x_i \sum w_i y_i\}/D \tag{33a}$$

$$I = \{\sum w_i x_i^2 \sum w_i y_i - \sum w_i x_i \sum w_i y_i\}/D \tag{33b}$$

and

$$D = \sum w_i \sum w_i x_i^2 - (\sum w_i x_i)^2 \tag{33c}$$

Finally, the slope value S is the negative of the activation energy E/R, and k_0, the pre-exponential or diffusion constant, is given by

$$k_0 = \exp(I) \tag{34}$$

The parameter w_i is the weight factor for each data point, given by $w_i = 1/\sigma_i^2$, where σ_i^2 is the variance in the y-dimension associated with the ith data point (Cvetanovic et al. 1979). For the functional form $y = \ln(r^2/t)$ it can be shown by the theory of propagation of errors that appropriate weight factors are given by $w_i = 1/((2CV_r)^2 + CV_t^2)$, where CV_r and CV_t are the coefficients of variation for r and t respectively (Cvetanovic et al. 1979; Taylor 1982: 179ff.).

For this analysis the value of CV_r is computed from the hydration rim values in microns measured by the laboratory. The value of CV_t is estimated from laboratory procedures, by assuming that the hot-soak time might vary from an exact number of days by up to an hour

or so due to heat-up and cool-down time, or about 0.05 days. The standard deviation of the uncertainty is then $0.05/\sqrt{(12)}$, which is then used in computing CV_t.

A final source of experimental error lies in the temperature controller for the laboratory oven used for the hot soak. Typical laboratory thermostat controllers are accurate to about ±1°C. It can be shown that this adds a temperature increment of 0.06°C to the nominal temperature of the controller; this increment is always positive, not random.

The linear best fit in equations (33a – c) provides best estimates for the mean values of activation energy (E), diffusion constant or pre-exponential (k_0), and hydration rate. Uncertainties associated with these mean values are characterized by the standard deviations of the activation energy and diffusion constant, which are, respectively,

$$\sigma_E = \sigma\{\textstyle\sum w_i/D\} \qquad (35)$$

and

$$\sigma_{k0} = A\sigma\{\textstyle\sum w_i\, x_i^2/D\} \qquad (36)$$

with D defined in equation (18c) and σ given by

$$\sigma = \{\textstyle\sum w_i(y_i - \hat{y}_i)^2/(N - 2)\}^{\frac{1}{2}} \qquad (37)$$

Here x and y are defined as above, $\hat{y}_i$ is the best-fit value of y_i computed from equations (6a-c), and N is the number of data points. The parameter σ is known as the "external or *a posteriori* standard deviation" (Cvetanovic et al. 1979:52).

Computation of the errors in hydration rate is more complicated. It cannot be simply inferred from σ_E and σ_{k0}, because there is also a strong cross-correlation term. If there were no cross-correlation, the standard deviation of the rate σ_{knc} would be simply

$$\sigma_{knc} = \sqrt{(\sigma_E^2 + \sigma_{k0}^2)} \qquad (38a)$$

Monte Carlo simulation studies have shown that the effect of the cross-correlation is to reduce the error in rate relative to equation (38), such that the error including cross-correlation σ_k is

$$\sigma_k \approx 0.57 \times \sigma_{knc.} \qquad (38b)$$

Laboratory Protocol:

A set of five specimens is prepared through percussion to generate a flake or by sectioning on a low-speed saw and polishing to a mirror finish. The same piece of obsidian should provide all of the samples. Each specimen is hydrated in a pressure vessel at a specific temperature for a defined length of time. At the end of the time, the pressure vessel is cooled rapidly with compressed air or water, the specimen removed, and the hydration rim measured. Hydration is performed either with distilled water (liquid phase hydration), or in a saturated water vapor atmosphere without liquid contact (vapor phase hydration). In liquid phase hydration the water contains a saturated solution of dissolved silica gel to prevent erosion of the glass surface. Temperatures employed in laboratory hydration typically range from 110 - 150°C; it has been found the going much over 150°C can lead to diffuse hydration. Hydration times typically range from ten days at the higher temperatures to thirty days or more at the lower temperatures in order to sure that well defined and easily observable hydration layers are present.

Two caveats apply to this method that are related to accuracy and reliability of the resulting rates. First, the accuracy of the method is surprisingly poor unless long hot-soak times are employed. This arises because of the form of equations (33a - c). The best-fit process generates a slope and y-intercept, the latter of which requires extrapolation from the measured values of 1/T to zero, which tends to amplify any errors in the data set. Further,

Temperature, °C	Hot soak time, days. Standard Protocol	Hot soak time, days. Recommended Protocol	Limiting factor
110	30	235	Achieving 5μ rim for a slow obsidian
120	25	120	Achieving 5μ rim for a slow obsidian
130	20	65	Achieving 5μ rim for a slow obsidian, and reaching steady state
140	15	60	Achieving steady state
150	10	55	Achieving steady state

Table 3. Hot-soak times for laboratory hydration

equation (34) involves raising the intercept value I to an exponential, which further amplifies errors. The errors in measuring the thickness of the hydration rims seem to be the dominant factor. The effect is reduced by extending the hydration period to achieve larger rims before making the readings. Measurement accuracies of $\approx 0.1\mu$ are typically reported by hydration laboratories, so a rim magnitude of 5μ yields a rim CV of 4%, or a rate CV 0f 10% (Rogers and Stevenson 2019: 123, Table 8) Thus, a rim magnitude greater than 5μ is desirable.

The second issue is more serious, and is related to the process of hydration. Hydration involves water molecules penetrating the glass matrix, which causes swelling of the hydrated layer. This swelling, or internal stress, is relieved by a relaxation process that involves a volumetric expansion of the glass, and is a function of glass viscosity (Rogers and Stevenson 2019: 122). The relaxation seems to be time-dependent, such that, at a single temperature, the apparent hydration rate varies with time and eventually reached steady state (Rogers and Duke 2014b: 433, Fig. 2, 434, Fig. 3; Stevenson and Novak 2011). This essentially invalidates equation (28), which is the basis of the method, so that measuring the hydration rim prior to that settling time gives invalid rates. Rogers and Duke (2014b) found that use of the standard hot-soak protocol yielded inaccurate results for six obsidians from southern Nevada; hydration rates were too large by approximately a factor of two, and the logarithmic Arrhenius plot showed a sigmoid

form instead of the expected straight line (Rogers and Duke 2014b: 433, Fig. 1).

Between the need to achieve a 5μ rim for a slow hydrating obsidian, and the time for relaxation to settle out, the hot-soak protocol recommended by Rogers and Stevenson (2017:120, Table 2) is as shown in Table 3. Relaxation time is not an issue with archaeologically-formed hydration rims, due to the long hydration times involved.

The resulting accuracy in rate is comparable to that achievable with radiocarbon association (Rogers and Stevenson 2017).

Intrinsic Water Calibration:

The hydration rate is known to be determined principally by the intrinsic water content of the obsidian (many references, e.g., Karsten and Delaney 1981; Karsten et al. 1982; Stevenson et al. 2000; Zhang et al. 1991; Zhang and Behrens 2000). Geochemical studies have led to equations for the hydration rate of obsidian in terms of temperature, pressure, and intrinsic water content (Zhang et al. 1991; Zhang and Behrens 2000). However, many analyses were based on temperatures (400 – 1200°C) and pressures (0.1 – 810 mPa) of interest to volcanology, and they do not extrapolate correctly to ambient archaeological temperatures.

Rogers (2015a) suggested a preliminary equation relating intrinsic water content and temperature to hydration rate for obsidian in the temperature and pressure ranges typical of archaeology. If intrinsic water content of the specimen is measured, either by IR spectrometry or by gravimetry, the hydration

rate can be estimated for any desired effective hydration temperature (EHT).

The analytic approach was, first, to develop the functional form of the equation from measurements of water mass increase in obsidian, based on data published by Stevenson and Novak (2011). Since the mass increase and the depth of penetration are two aspects of the same phenomenon, the general form of the model should be similar. The second step was to adapt the model to optical measurement by adjusting the numerical value of the parameters, based on data from the obsidian flows in the Coso volcanic field in Inyo County, California. The resulting equation is

$$k=\exp(37.76-2.289w_s-10433/T+1023w_s/T) \quad (39)$$

Here w_s is total intrinsic water in wt %, T is effective hydration temperature in °K, and k is hydration rate in $\mu^2/1000$ yrs. The factor 37.76 is simply a scale factor; 2.289/wt%, expresses a temperature-independent variation with water concentration; 10433°K is the basal activation energy of dry obsidian; 1023°K/wt%, represents the variation of activation energy with both temperature and water concentration. A major caveat is that equation (39) was developed based on a very small data set of six samples, so it must be used with caution.

Use of equation (39) requires knowing w, the intrinsic water content. Measurement techniques for water content is beyond the scope of this paper; spectroscopic methods include Fourier Transform Infrared (FTIR) spectrometry (e.g. Newman et al. 1986; Von Aulock 2014), Infrared Photo-Acoustic Spectrometry (IR-PAS; Stevenson and Novak 2011). An alternative method based on gravimetry, or Archimedes' Principle, is described in Stevenson et al. (2018).

Curve Re-Fitting:

If a best-fit curve is available which does not conform to the known physics discussed here, and if the data from which it was developed are not available, the curve can be re-analyzed to provide a rate based on square-root-of-time principles. Describing the method is best done by example.

Basgall and Giambastiani (1995:44) analyzed Queen obsidian artifacts from the Bishop Tablelands area, and computed a best fit equation of

$$t = 82.74 * r^{2.06} \quad (40)$$

where t is age in radiocarbon years before the present (rycbp, with "the present" understood as 1950) and r is hydration rim in microns. This equation was apparently the result of a linear best fit to obsidian-radiocarbon data pairs, in which the fit was between ln(t) and ln(r). However, the fit does not recognize the physics of the process. Hydration is a diffusion process, and hence, by definition, the exponent in the right side of the equation must be equal to 2, so that equation (1) above applies. The original data set was not published by the researchers, so our re-analysis is based on equation (40).

The analytical procedure was to select a set of hydration rim readings and compute the corresponding age by equation (39).The rim values should be selected to span the likely range of values in the archaeological sample. The ages were then converted to calibrated years before 1950 (cyb1950) using Calib 6.0, and 50 years was added to adjust to the year 2000 (cyb2k). Finally, a linear least-squares best fit was made between r^2 (independent variable) and t in cyb2k (dependent variable). Table 4 presents the data used.

The linear best fit constrained to pass through the origin yields a slope of 114.57 yrs/μ^2. The rate is the reciprocal of the slope, or 8.73 $\mu^2/1000$ years. The EHT for the area was computed by regional temperature scaling to be 18.59°C; adjusting the rate to 20°C yields a rate of 10.34 $\mu^2/1000$ years.

In this case the results agree with other methods (Rogers and Stevenson 2019); again, however, the method should be used with care and frequent cross-checking.

rim, μ	t, rcybp	t, cyb1950	rim ^{2}, μ^2	t, cyb2k
2	345	398	4	448
4	1439	1353	16	1403
6	3317	3558	36	3608
8	5999	6850	64	6900
10	9500	10824	100	10874
12	13830	16927	144	16977
14	18999	22621	196	22671

Table 4. Queen obsidian data, Bishop Tablelands.

Inter-Method Proportionality:

This method was developed to compensate for non-equilibrium conditions in certain laboratory induced hydration protocols, as described above and in Rogers and Duke (2014b). A ratio is computed between the non-equilibrium rate and an archaeological rate. It is then applied to correct other laboratory induced hydration rates computed from the same lab protocol, for which archaeological rates are not available. Again, a specific example will be shown.

Rogers and Duke (2014b) reported hydration rates based on laboratory hydration for obsidian from seven Lincoln County, Nevada, obsidian sources: Meadow Valley Mountains, Delamar Mountains, Panaca Summit, Tempiute Range, Clover Mountains, Wilson Creek Range, and South Pahroc. Hydration rates were also computed based on projectile point data from the Kern River Pipeline for the first three of these sources. The results are in Table 5 (Rogers and Duke 2014b: 433, Table 5).

Further analysis showed that all the induced rates are too high. However, the ratio between archaeological rate and induced rate for the first three sources is very close to the same: for Meadow Valley Mountains it is 0.53, for Delamar Mountains it is 0.57, and for Panaca Summit it is 0.51. The CVs for these rates are large, so the ratios are not statistically distinguishable and we are justified in using the average of 0.54. Thus, the missing archaeological rates can be reconstructed by multiplying the induced rate by 0.54. The physics involved appears to be consistent. In each case the induced hydration rate is clearly not representative of equilibrium conditions, and the logarithmic Arrhenius plots all showed the sigmoid indicating that the relaxation had not reached equilibrium condition under the protocol used. The induced rate is probably the result of an interaction between a transient phenomenon (onset of accelerated hydration at an elevated temperature) and the particular experimental protocol employed. Since all the specimens were subjected to the same protocol

Source	Induced Rate, μ^2/1000 yrs at 20°C	Archaeological Rate μ^2/1000 yrs at 20°C
Delamar Mountains	31.9	18.3, N = 12
Meadow Valley Mountains	24.3	12.8, N = 27
Panaca Summit	30.2	15.3, N = 93
Tempiute Range	33.8	na
Clover Mountains	19.7	na
Wilson Creek Range	15.2	na
South Pahroc	16.2	na

Table 5. Laboratory and archaeological data for Nevada sources

Source	Rate, μ^2/1000 yrs at 20°C	CV	Comments
Delamar Mountains	18.3	0.37	Archaeological
Meadow Valley Mountains	12.8	0.13	Archaeological
Panaca Summit	15.3	0.13	Archaeological
Tempiute Range	18.1	0.2 (assumed)	Scaled from induced rate
Clover Mountains	10.6	0.2 (assumed)	Scaled from induced rate
Wilson Creek Range	8.1	0.2 (assumed)	Scaled from induced rate
South Pahroc	8.6	0.2 (assumed)	Scaled from induced rate

Table 6. Scaled hydration rate data.

by the lab, the response of the obsidian specimens should be consistent across the various sources, at least to first order. The fact that the ratios agree so closely for the first three is probably not an accident. Applying this method to the remaining four sources yield the rates in Table 6.

Age Accuracy

There are always errors, or uncertainties, in the parameters used for age computation. In obsidian hydration dating the primary error sources are: obsidian rim thickness measurement; errors in the hydration rate ascribed to a source; intra-source rate variability due to uncontrolled intrinsic water in the obsidian (Ambrose and Stevenson 2004; Rogers 2008a, 2010; Stevenson et al. 1993, 2000; Zhang et al. 1991; Zhang and Behrens 2000); errors in reconstructing the temperature history (EHT); uncertainties due to humidity variations; and association errors caused by site formation processes (Schiffer 1987).

Obsidian sample sizes are generally relatively small due to cost constraints, typically 8-10 specimens, while the uncertainty sources described above produce at least six degrees of freedom in the errors. For this reason, sample standard deviation is generally not a good estimate of age accuracy; a better
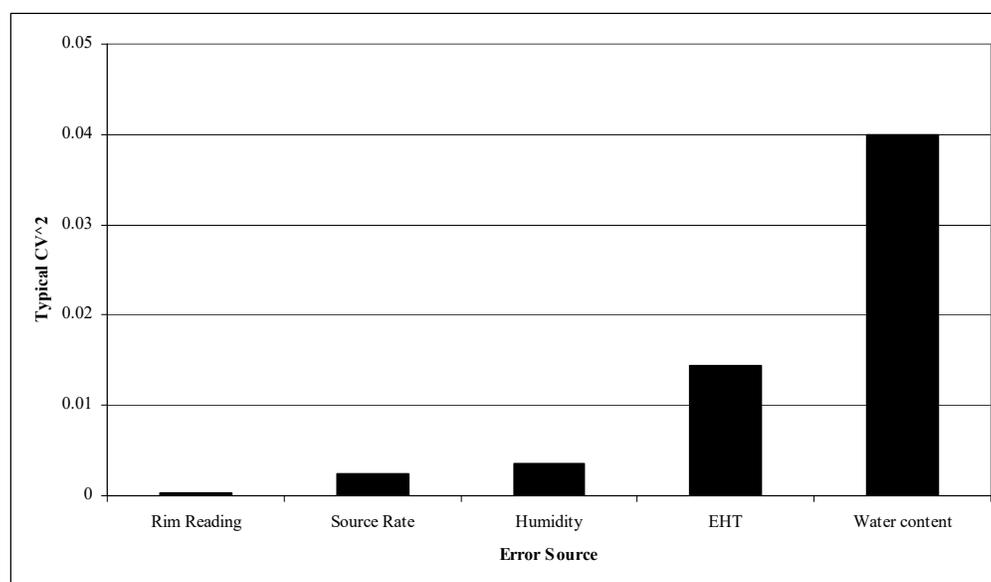
Figure 8. Typical relative magnitudes of error sources in OHD. Note that intrinsic water variation and temperature history (EHT uncertainty are the major contributors.

State	Geochemical Source	Rate*	Rate CV	Method*	Confidence	Remarks
CA	Coso volcanic field (composite)	22.86	0.33	2	H	
CA	Coso West Sugarloaf	18.14	0.20	1, 4	H	
CA	Coso Sugarloaf Mountain	29.87	0.13	1, 4	H	
CA	Coso West Cactus Peak	27.28	0.37	4	H	
CA	Coso Joshua Ridge	22.27	0.26	4	H	
CA	Casa Diablo Lookout Mountain	13.04	0.15 (est)	5	M	Small sample
CA	Casa Diablo Sawmill Ridge	12.70	0.15 (est)	5	M	Small sample
CA	Bodie Hills	10.85	0.09	4	H	
CA	Fish Springs	11.87	0.15 (est)	5	M	Small sample
CA	Mono Glass Mountain	9.97	0.15 (est)	4	M	
CA	Mono Craters	33.00	0.15 (est)	4	H	
CA	Saline Range	9.95	0.15 (est)	4	M	
CA	Eureka Dunes	9.95	0.15 (est)	4	M-L	Small sample
CA	Napa Glass Mtn	10.68	0.10	1	H	
CA	Obsidian Butte (Salton Sea)	9.09	0.15 (est)	2	M	
NV	Truman-Queen	10.50	0.15 (est)	6	H	
NV	Mt. Hicks	11.79	0.15(est)	4	M	
NV	Delamar Mountains	18.32	0.37	1,3	H	
NV	Panaca Summit	15.22	0.13	1,3	H	
NV	Meadow Valley Mountains	12.79	0.13	1,3	H	
NV	Tempiute Range	18.10	0.2 (est)	7	M-L	
NV	Clover Mountains	10.60	0.2 (est)	7	M-L	
NV	Wilson Creek Range	8.10	0.2 (est)	7	M-L	
NV	South Pahroc	8.60	0.2 (est)	7	M-L	
UT	Topaz Mountain	8.14	0.28	1, 2	H	
UT	Brown's Bench	15.16	0.15 (est)	2, 4	H	

Table 7. Provisional hydration rates (um^2/1000 years) for obsidian sources in eastern California at 20 deg. C. * 1 = laboratory induced hydration, 2 = radiocarbon association, 3 = temporally-sensitive artifact association, 4 = intrinsic water calibration, 5 = artifact baselining, 6 = curve re-fitting, 7 = inter-method proportionality.

strategy for estimating age accuracy is to use *a priori* information about the individual error sources, and infer the accuracy of the age estimate. The mathematics to make this inference were developed in Rogers (2010), and are summarized here.

The coefficient of variation of the computed age estimate, CV_t, can be shown to be

$$CV_t^2 = 4*(\sigma_r/r)^2 + (0.12\sigma_{EHT})^2 + CV_{ks}^2 + CV_{ke}^2 + CV_{hum}^2 \quad (41)$$

where the variables are defined as follows: σ_r is the standard deviation of the hydration rim measurement, and is $\approx 0.1\mu$; r is the mean hydration rim; σ_{EHT} is the standard deviation in EHT post-correction, and is $\approx 1.0°C$; CV_{ke} is

the coefficient of variation of the hydration rate ascribed to the obsidian source, and is typically ≈ 0.05; CV_{ks} is the coefficient of variation of rate due to intra-source rate variations, with typical CV values as in Table 7; CV_{hum} is the coefficient of variation of rate due to humidity variations and ≈ 0.06. Figure 8 shows the relative magnitudes of the terms in equation (41), and shows that the intrinsic water variability is by far the largest contributor to age uncertainty, followed by uncertainty in EHT.

If the provenience is such that site formation uncertainties must be included, VAR_{SF}, the variance of age due to site formation is

$$VAR_{SF} = (t_d - t_s)^2/12 \quad (42)$$

where t_d is the age computed for burial depth conditions and t_s is the age computed for surface conditions.

Once CV_t is computed from equation (40), the standard deviation of the uncertainty in the age estimate is

$$\sigma_t = \text{sqrt}[t \times CV_t^2 + VAR_{sf}] \tag{43}$$

This is the accuracy figure quoted in the computer program output.

The best measure of the uncertainty associated with OHD ages from a sample of size N, with individual ages and age standard deviations (SD_{age}), is the probable error of the means, taking into account both the variation in the mean ages making up the sample and their corresponding values of SD_{age}. This parameter, U_a, is given by

$$U_a = \text{sqrt}(SD_m^2 + B^2)/\text{sqrt}(N) \tag{44}$$

where SD_m is the standard deviation of the means, B is the average of the individual specimen variances ($= \Sigma SD_{age}^2/N$), and N is sample size.

Hydration Rates Listing

Hydration rates are continually being refined as techniques improve, so the rates shown in Table 7 should be regarded as provisional. The analyst should always check on whether the rate employed is giving an archaeologically result that converges with other chronometric information.

Analytical Procedure

The Obsidian Hydration Dating Process:

Here we describe a recommended process for performing an OHD analysis. The discussion pulls together the mathematics from the preceding text, with practical suggestions for the analysis.

To begin with, the analyst will need the following data to perform an OHD analysis. First, to perform the computations themselves,

site elevation (feet above mean sea level) and specimen burial depth (cm below the surface) are needed for computation of EHT. The geochemical source of each specimen is needed to match with the hydration rate, and the hydration laboratory report giving rim mean and standard deviation is needed for the age computation. The hydration laboratory comments about hydration layer clarity and thickness variation are especially helpful in evaluating the results and explaining anomalous ages. Next, site nomenclature (trinomial or temporary number) and provenience of each specimen (TU, level, other designation) are needed to report results in a coherent fashion. Tentative identification of each artifact (such as biface, debitage, projectile point) is desirable. Furthermore, if any of the specimens are temporally sensitive, such as projectile points, it is useful to know the typology as a means to cross-check the OHD ages.

Data Preparation:

The following are general guidelines for efficient analysis of obsidian hydration data. As always, exceptions may be made depending on circumstances.

1. Always use geochemical methods to determine obsidian source. Visual sourcing cannot generally identify subsources, which may have different hydration rates. If geochemical sourcing was not performed, clearly state the sourcing assumptions made.
2. Group hydration data by geochemical source – never mix sources.
3. Treat obvious tools, such as projectile points or crescents, as individual items (N = 1). For the rim standard deviation, use the value reported by the lab.
4. Debitage samples with N > 1 may be treated individually or grouped by provenience and burial depth.
5. The hydration rim mean reported by the laboratory is usually the average of six independent readings made on a thin-

section, and the reported standard deviation is computed from those six readings. Most labs provide these data in an Excel spreadsheet, with formatting set to round off to one decimal place. It is important to change the formatting to show the standard deviation to three decimal places for the accuracy computation.

6. Tabulate the rim means, standard deviations, burial depths, and geochemical sources for use in the analysis. Explain the rationale for any grouping of data, and especially for any data points excluded (whether by Chauvenet's criterion or judgmentally).

Analysis Procedure:

The recommended procedure for chronometric analysis is to proceed by the following steps. All temperatures are in °C, and cyb2k means "calibrated (or calendar) years before 2000".

1. Compute the site temperature parameters from meteorological records or sensors. A temperature model such as described in Table 2 is a convenient means to do this. If any specimen is from a rock shelter or cave, multiply V_a by 75% and use $V_d = 5°C$.
2. Make sure all the specimens are matched with the appropriate hydration rate for the geochemical source.
3. Using the temperature parameters from step 1 and the burial depth z in meters, compute the EHT for each specimen by numerical integration of equation (10) or by using equations (11) and (12).
4. If using MatLab, compute E/R by equation (14); otherwise set E/R = 10000.
5. Compute the EHT-corrected rim thickness for each specimen by equations (13) and (15).
6. Compute ages based on current conditions using equation (1) and the appropriate rate from Table 7.
7. Once the ages are known, compute the age standard deviation from equation (41).
8. If the site morphology is such that site

formation processes need to be taken into account, repeat the computations and determine the age assuming surface conditions (z = 0). Then compute the age variance for site formation from equation (42) and the overall age uncertainty from equation (43).

Computation Using MatLab:

The analysis code in Appendix A is written in MatLab 7.0, and is compatible with earlier versions of MatLab back to 5.0. The EHT is computed by numerical integration, and age and age standard deviation are computed. The code is fully documented with internal comments, and the variable names are, as far as possible, mnemonic. The code reads input from an MS Excel-generated comma-separated variable (.csv) file, and outputs to a similar file. The user must generate in input files, using MS Excel or equivalent. The names on the input and output files may be adjusted by the user. The code and its design are fully documented in Rogers 2018a.

Computation Using MS Excel Workbook:

An MS Excel workbook has been developed which follows the procedure outlined above. Layout of the workbook is shown in Appendix C, with the parameter definitions in Table 8.

The data in columns A – D in the workbook can be simply copied from the electronic worksheet provided by the obsidian laboratory, and pasted into the workbook. By constructing the workbook with the equations incorporated in the second row (first row of data), the age computation is then carried out by a simple <fill down> procedure in MS Excel. The advantage of such a layout is that it facilitates checking the results, as mistakes show up clearly.

Data Presentation:

In presenting OHD results in a report, always report complete data on the obsidian

Column	Parameter	Parameter definitions	Source
A		Specimen number	Assigned by user
B	R_m	Measured hydration rim, microns	Lab report
C	SD_m	Standard deviation of rim reading, microns	Lab report
D	z	Burial depth, cm below surface	Lab report
E	Source	Geochemical source of specimen	Lab report
F	Rate	Hydration rate corresponding to the geochemical source, microns^2/1000 yrs.	User entry from Table 7 or other source
G	Rate CV	CV of the hydration rate due to intrinsic water content.	User entry from Table 7 or other source
H	Rate EHT	Effective hydration temperature corresponding to the rate value.	User entry from Table 7 or other source
I	T_a	Surface annual average temperature at the site	User entry from meteorological records or sensors
J	V_{a0}	Surface annual variation in temperature (hottest-month mean minus coldest-month mean)	User entry from meteorological records or sensors
K	V_{d0}	Surface mean diurnal temperature variation at the site	User entry from meteorological records or sensors
L	V_a	Annual temperature variation at artifact burial depth	Equation 11a
M	V_d	Mean diurnal temperature variation at artifact burial depth	Equation 11b
N	EHT	Effective hydration temperature at artifact burial depth	Equation 12a,b
O	RCF	Rim correction factor	Equation 13
P	R_c	Rim adjusted to same EHT as the hydration rate	Equation 15a
Q	SD_r	EHT-adjusted rim standard deviation	Equation 15b
R	Age CV	CV of age estimate*	Equation 41
S	Age	Age of artifact, cyb2k	Equation 1
T	Age SD	Standard deviation of age	Equation 43

Table 8. Definitions for Excel Workbook.
* Constant values used in equation 40: CV hum = 0.06; CV EHT = 0.12; CV Rate = 0.05; other parameters computed from input data.

hydration samples. This should include catalog number or other identifier; a description of the artifact, such as debitage or biface; the mean and standard deviation for each rim; the obsidian source and how it was determined; provenience, including unit designation and burial depth; any unusual circumstances, such as cave or hearth; the EHT-corrected rim means and standard deviations; and the computed mean and standard deviation of the age, in cyb2k. The site description should always include site elevation.

Data may be aggregated by unit, level, or other convenient basis, depending on the context of the site. Anomalous ages should be addressed in the text to aid in interpretation.

In analyzing archaeological data, it is often desirable to group dates by archaeological period in histogram format. Typically ages are assigned to periods simply by "binning", placing the mean value into a period "bin". If standard deviation of the age is small, this can be a reasonable method; however, if standard deviation is large it can lead to ambiguities, since a date near a period boundary could be assigned to either period with nearly equal probability (Figure 9). This is a particular issue
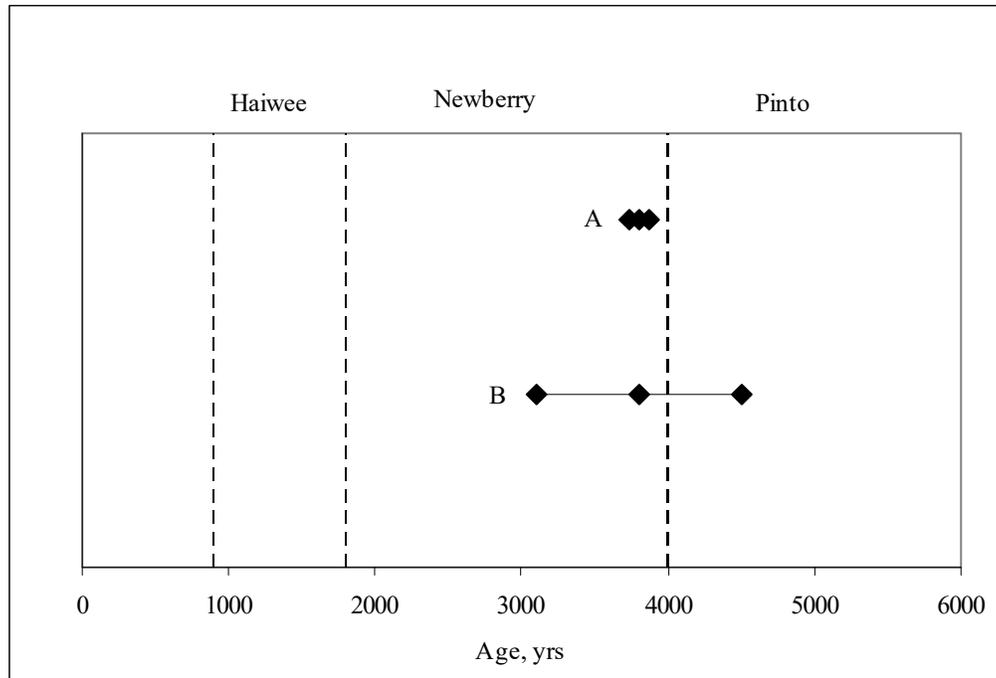
Figure 9. The "binning" problem. Mean and standard deviation are shown for the two specimens. Specimen A can safely be assigned to the Newberry period, while specimen B can fall into either the Pinto or Newberry periods with almost equal probability.

for obsidian hydration dating, since the standard deviations tend to be large.

For obsidian hydration dating, the mean and standard deviation of age define a normal (Gaussian) probability curve, so a more rigorous method of ascribing dates to archaeological periods is to compute the area under the probability curve within each period (Figure 10).

The mathematical method is, given a mean and standard deviation, to compute the $P(L_n, L_{n+1})$, the probability that the age lies between ages L_n and L_{n+1}, where L_n and L_{n+1} are the limits of an archaeological period:

$$P(L_n, L_{n+1}) = erf(L_{n+1}) - erf(L_n) \qquad (45)$$

Here erf(x) is the error function, defined as the integral of the normal curve from $-\infty$ to x. The function is readily available in both MS Excel and MatLab without programming. After computing $P(L_n, L_{n+1})$ for each artifact and each archaeological period bin, the probabilities are

summed for each bin. A MatLab code implementing this grouping is in Appendix B; results can be converted to histogram by MS Excel.

Status and Outlook for the Future

It has been nearly 60 years since the original obsidian hydration dating work of Friedman and his colleagues and their work has stood the test of time. They correctly identified the physical process involved (diffusion) and the mathematical form of the hydration law (equation [1] above); they also pointed out, based on physical chemistry, that the diffusion coefficient must be concentration-dependent in order to create a hydration rim. And finally, to their credit, they realized the importance of grouping obsidian by geochemical source, and the effects of temperature and humidity. In succeeding years other researchers, primarily in glass science and geochemistry, developed the field further. The archaeological advances over the past decade, which are the subject of
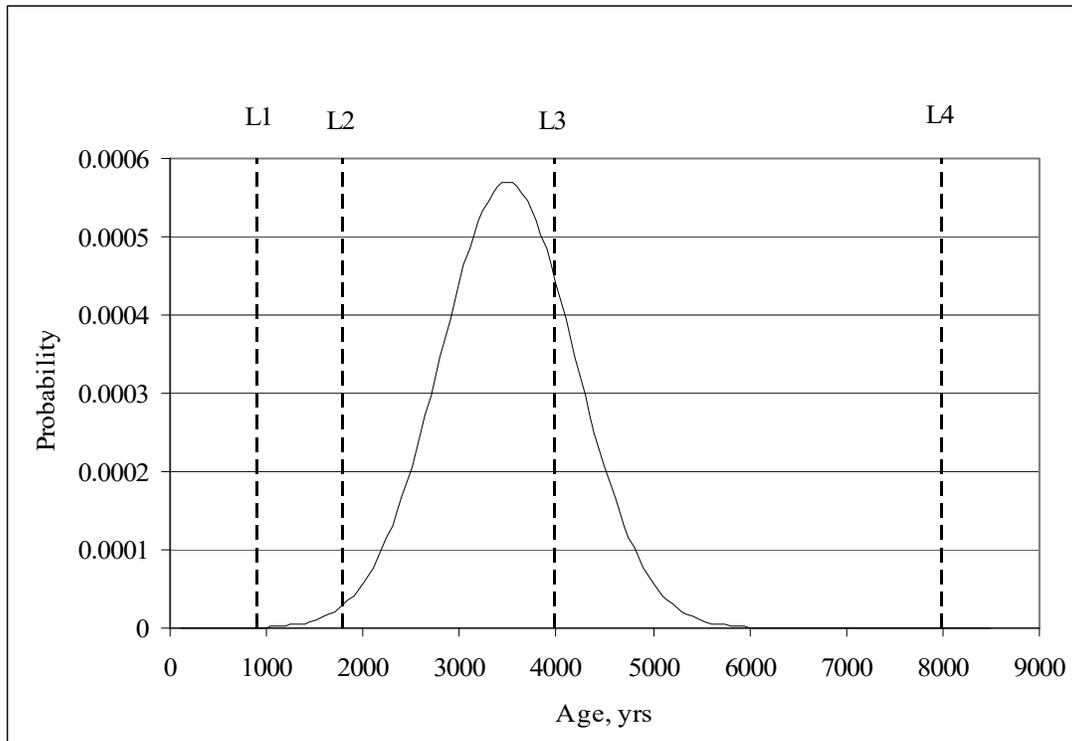
Figure 10. The "binning" problem, illustrating the computation in equation (43). The erf(x) is the area under the curve.

this paper, have been chiefly the result of applying numerical modeling to the known physical and chemical basis of hydration. At present the mechanism of hydration is well understood at a macro level, and can be successfully applied to archaeological problems. Current models enable computing both an age and a standard deviation of the age, and sources of uncertainty contributing to the standard deviation are known.

There are limitations to the OHD method. We have effective first-order OHD models for effects of intrinsic water, temperature, and humidity. The primary limitations to OHD accuracy and precision occur because these models are generally not developed for the specimen but for the environment. For example, the temperature model is developed for the site and burial depth, but not for the specific obsidian specimen, and humidity can only be accounted for statistically. Similarly, hydration rates are computed for geochemical

sources, but do not account for the intrinsic water in a particular obsidian artifact; further, they are subject to potential error sources such as the obsidian-radiocarbon association uncertainty. As a result, OHD dates typically have relatively poor precision (age uncertainties of ~ 15 - 25%). Given this "open-loop" nature of the modeling process, it is unlikely that further refinement of the present process will lead to dramatic improvements in precision as long as the sources of uncertainty remain unresolved.

Looking to the future, there are four areas of research which promise significant improvements. The first is a method for measuring the intrinsic water content of the individual specimen, cheaply, quickly, and without damage to the specimen. Such a method would enable the hydration rate to be computed for the individual artifact rather than being ascribed to the geochemical source, and would lead to a dramatic improvement in age

precision. In equation (41), CV_{ks} was defined as the rate CV due to intra-source variations in intrinsic water, and is by far the dominant error source as shown in Figure 8 above. To reduce CV_{ks} to the same magnitude as that for the rate ascribed to the obsidian source requires CV_{ks} of ≈ 0.05, which would require measuring the water content itself to within 0.02 wt%. Analysis of the Beer-Lambert law method of Newman et al. (1986) indicates that such accuracies are feasible with FTIR measurement techniques (Rogers 2016).

A second promising improvement would be a method to determine the temperature history an artifact has experienced by a measurement on the artifact itself, or "intrinsic EHT". A possible phenomenon is the water speciation process. As molecular H_2O diffuses into the glass, some fraction reacts with the glass matrix and becomes hydroxyl (OH), a process known as speciation. The process is slow, and the fraction which reacts is a function of temperature; thus, the fraction of total water which has become OH is a measure of the temperature history. However, the currently-published equation relating OH fraction to temperature was derived for geologic temperatures and pressures, and it is not certain the equation applies to archaeological conditions. Further, the temperature thus derived would need to be accurate to within 1°C, and current measurement methods are destructive to the specimen. Much more research is needed in this area.

A third area for research is to develop a quantitative understanding of hydration at the molecular level. The present models, based on diffusion coupled with chemical reaction, are macro-level, phenomenological models. They are based on understanding and including molecular-level effects, but the models themselves are higher-level. The mathematical models of diffusion were first developed in the early 19th century by Laplace, specifically for describing heat transfer in solids; they were subsequently applied to mass transfer by Fick (Crank 1975). For the case of diffusion without reaction and with a constant diffusion coefficient (D in equation [2]) the same results can be derived at the molecular level by kinetic theory (Glicksman 2000:191ff.). This corresponds physically to diffusion of one gas into another without chemical reaction. However, for the more complex case of diffusion with reaction, such a model does not exist. Kuroda et al. (2018) have developed a model at temperatures of 650 – 850°C and pressures of 50 bar, but it is not clear that the data extrapolate to archaeological conditions. The goal of research in this area would be a mathematical model which starts with the structure and composition of the glass matrix and allows computing both a hydration rate and the speciation reaction.

A final area of research is much less glamorous, but is sorely needed: a method for measuring the hydration rim without damage to the artifact. Current methods require cutting a small piece of obsidian from the margin of an artifact, and land-management agencies are increasingly unwilling to allow damage to artifacts. In some cases the notch can be replaced by the unobtrusive removal of a pressure flake, but this still qualifies as "damage", as does the micron-size pit created by SIMS. The method would need to be fast, cheap, non-damaging, and applicable to a wide range of artifact types and sizes. A method meeting these criteria does not currently exist.

Note: References from the *International Association for Obsidian Studies Bulletin* are available to download from the web site, http://www.deschutesmeridian.com/IAOS/bulletin.html

References Cited

Ambrose, W. R., and C. M Stevenson (2004) Obsidian Density, Connate Water, and Hydration Dating. *Mediterranean Archaeology and Archaeometry* 4(2): 5-16.

Anovitz, L. M., J. M. Elam, L. R. Riciputi, and D. R. Cole (1999) The Failure of Obsidian Hydration Dating: Sources, Implications, and New Directions. *Journal of Archaeological Science* 26(7): 735-752.

Anovitz, L. M., J. M. Elam, L. R. Riciputi, and D. R. Cole (2004) Isothermal Time-Series Determination of the Rate of Diffusion of Water in Pachuca Obsidian. *Archaeometry* 42(2): 301-326.

Anovitz, L. M., D. R. Cole, and M. Fayek (2008) Mechanisms of Rhyolitic Glass Hydration Below the Glass Transition. *American Mineralogist* 93: 1166-1178.

Basgall, M. E. (1990) *Hydration Dating of Coso Obsidian: Problems and Prospects*. Paper presented at the 24th Annual Meeting of the Society for California Archaeology, Foster City.

Basgall, M., and M. Giambastiani (1995) *Prehistoric Use of a Marginal Environment: Continuity and Change in Occupation of the Volcanic Tablelands, Inyo and Mono Counties, California*. Center for Archaeological Research at Davis, California.

Behrens, H., and M. Nowak (1997) The Mechanisms of Water Diffusion in Polymerized Silica Melts. *Contributions to Mineralogy and Petrology* 126: 377-385.

Bintanja, R., R.S.W. van de Wal, and J. Oerlemans (2005) Modelled Atmospheric Temperatures and Global Sea Levels over the Past Million Years. *Nature* 437: 125-128.

Carslaw, H. S., and J. C. Jaeger (1959) *Conduction of Heat in Solids*, 2nd ed. Clarendon Press, Oxford.

Cole, F. W. (1970) *Introduction to Meteorology*. Wiley, New York.

Crank, J. (1975) *The Mathematics of Diffusion*. Oxford University Press, Oxford.

Cvetanovic, R. J., D. L. Singleton, and G. Paraskevopoulos (1979) Evaluations of the Mean Values and Standard Errors of Rate Constants and their Temperature Coefficients. *Journal of Physical Chemistry* 83(1): 50-60.

Delaney, J. R., and J. L. Karsten (1981) Ion Microprobe Studies of Water in Silicate Melts: Concentration-Dependent Water Diffusion in Silicon. *Earth and Planetary Science Letters* 52: 191-202.

Doremus, R. H. (1994) *Glass Science*, 2nd. ed. Wiley Interscience, New York.

Doremus, R. H. (2000) Diffusion of Water in Rhyolite Glass: Diffusion-reaction Model. *Journal of Non-Crystalline Solids* 261(1): 101-107.

Doremus, R. H. (2002) *Diffusion of Reactive Molecules in Solids and Melts*. Wiley Interscience, New York.

Ebert, W. L., R. F. Hoburg, and J. K. Bates (1991) The Sorption of Water on Obsidian and a Nuclear Waste Glass. *Physics and Chemistry of Glasses* 34(4): 133-137.

Everett-Curran, L., R. G. Milo, and D. Quiatt (1991) Microgeographic Comparisons of Climate Today Afford Inferences Concerning Past Behavior: An Overview of Data and Applications from a Study of Chapin Mesa (Mesa Verde National Park) Climate. In *Anasazi Symposium 1991*, edited

by A. Hutchinson and J. E. Smith, pp. 109-116. Mesa Verde Museum Association, Colorado.

Friedman, I., and R. Smith (1960) A New Method of Dating Using Obsidian; Part 1, the Development of the Method. *American Antiquity* 25 (4): 476-522.

Friedman, I., and W. Long (1976) Hydration Rate of Obsidian. *Science* 191(1): 347-352.

Friedman, I., R. I. Smith, and W. D. Long (1966) Hydration of Natural Glass and Formation of Perlite. *Geological Society of America Bulletin* 77: 323-328.

Friedman, I., F. W. Trembour, F. I. Smith, and G. I Smith (1994) Is Obsidian Hydration Dating Affected by Relative Humidity? *Quaternary Research* 41(2): 185-190.

Hughes, R. E. (1988) The Coso Volcanic Field Reexamined: Implications for Obsidian Sourcing and Dating Research. *Geoarchaeology* 3: 253-265.

Johnson, M. J., C. J. Mayers, and B. J. Andraski (2002) *Selected Micrometeorological and Soil-Moisture Data at Amargosa Desert Research Site in Nye County near Beatty, Nevada, 1998 – 2000.* U.S. Geological Survey Open-File Report 02-348. USGS, Carson City, Nevada. With CD containing meteorological data records.

Justice, N. D. (2002) *Stone Age Spear and Arrow Points of California and the Great Basin.* Indiana University Press, Bloomington.

Karsten, J. R., and J. L. Delaney (1981) Ion Microprobe Studies of Water in Silicate Melts: Concentration-Dependent Water Diffusion in Obsidian. *Earth and Planetary Science Letters* 52: 191-202.

Karsten, J. L., J. R. Holloway, and J. L. Delaney (1982) Ion Microprobe Studies of Water in Silicate Melts: Temperature-Dependent Water Diffusion in Obsidian. *Earth and Planetary Science Letters* 59: 420-428.

Kuroda, M., S. Tachibana, N. Sakamote, S. Okumura, M. Nakamura, and N. Yuimoto (2018) Water Diffusion in Silica Glass through Pathways formed by Hydroxyls. *American Mineralogist* 103: 412-417.

Lapham, K. E., J. R. Holloway, and J. R. Delaney (1984) Diffusion of H_2O and D_2O in Obsidian at Elevated Temperatures and Pressures. *Journal of Non-Crystalline Solids* 67: 179-191.

Liritzis, I., and N. Laskaris (2012) The SIMS-SS Obsidian Hydration Dating Method, In *Obsidian and Ancient Manufactured Glasses*, edited by I. Liritzis and C. M. Stevenson, pp. 26-45. University of New Mexico Press, Albuquerque.

Mazer, J. J., C. M. Stevenson, W. L. Ebert, and J. K. Bates (1991) The Experimental Hydration of Obsidian as a Function of Relative Humidity and Temperature. *American Antiquity* 56(3): 504-513.

Meyer, S. (1975) *Data Analysis for Scientists and Engineers.* Wiley, New York.

Michels, J. W. and Bebrich, C. A. (1971) Obsidian Dating. In *Dating Techniques for the Archaeologist*, edited by H. N. Michael and E. K. Ralph, pp. 164-221. MIT Press, Cambridge.

Morgenstein, M. E, C. L. Wickett, and A. Barkett (1999) Considerations of Hydration-rind Dating of Glass Artefacts: Alteration Morphologies and Experimental Evidence of Hydrogeochemical Soil-zone Pore Water Control. *Journal of Archaeological Science* 26: 1193-1210.

Newman, S., Stolper, E. M., Epstein, S. (1986) Measurement of Water in Rhyolitic Glasses: Calibration of an Infrared Spectroscopic Technique. *American Mineralogist* 71: 1527-1541.

Pearson, J. L. (1995) *Prehistoric Occupation at Little Lake, Inyo County, California: A Definitive Chronology.* Unpublished MA thesis, Department of Anthropology, California State University, Los Angeles.

Riciputi, L. R., J. M. Elam, L. M. Anovitz, and D. R. Cole (2002) Obsidian Diffusion Dating by Secondary Ion Mass Spectrometry: A Test Using Results from Mound 65, Clalco, Mexico. *Journal of Archaeological Scienc*e 29: 1055-1075.

Ridings, R. (1996) Where in the World Does Obsidian Hydration Dating Work? *American Antiquity* 61(1): 136-148.

Rogers, A. K. (2007a) Effective Hydration Temperature of Obsidian: A Diffusion-Theory Analysis of Time-Dependent Hydration Rates. *Journal of Archaeological Science* 34: 656-665.

Rogers, A. K. (2007b) A Tale of Two Gophers: Depth Correction for Obsidian Effective Hydration Temperature in the Presence of Site Turbation Effects. *International Association for Obsidian Studies Bulletin* 37: 7-12.

Rogers, A. K. (2008a) Obsidian Hydration Dating: Accuracy and Resolution Limitations Imposed by Intrinsic Water Variability. *Journal of Archaeological Science*. 35: 2009-2016.

Rogers, A. K. (2008b) Field Data Validation of an Algorithm for Computing Effective Hydration Temperature of Obsidian. *Journal of Archaeological Science*. 35: 441-447.

Rogers, A. K. (2008c) An Evaluation of Obsidian Hydration Dating as a Chronometric Technique, Based on Data from Rose Spring (CA-INY-372), Eastern California. *International Association for Obsidian Studies Bulletin* 40: 12-32.

Rogers, A. K. (2010) Accuracy of Obsidian Hydration Dating based on Radiocarbon Association and Optical Microscopy. *Journal of Archaeological Science*. 37: 3239-3246.

Rogers, A. K. (2011) Do Flow-Specific Hydration Rates Improve Chronological Analyses? A Case Study for Coso Obsidian. *International Association for Obsidian Studies Bulletin* 45: 14-25.

Rogers, A. K. (2012a) Temperature Correction for Obsidian Hydration Dating, In *Obsidian and Ancient Manufactured Glasses*, edited by I. Liritzis and C. M. Stevenson, pp. 46-55. University of New Mexico Press, Albuquerque.

Rogers, A. K. (2012b) Estimation of Hydration Rate for Casa Diablo and Fish Springs Obsidians from Tulare Lake Projectile Point Data. Maturango Museum working Manuscript MS109, dated July 1, 2012.

Rogers, A. K. (2015a) An Equation for Estimating Hydration Rate of Obsidian from Intrinsic Water Concentration. *International Association for Obsidian Studies Bulletin* 53: 5-13.

Rogers, A. K. (2015b) A Method for Correcting OHD Age for Paleo-temperature Variation. *International Association for Obsidian Studies Bulletin* 52: 6-13.

Rogers, A. K. (2016) Measurement of Water Content by Beer's Law. Maturango Museum working Manuscript MS172, dated Feb. 17, 2016.

Rogers, A. K. (2017) Steady-State Hydration and Protocols for Induced Hydration of Obsidian. *International Association for Obsidian Studies Bulletin* 57: 7-12.

Rogers, A. K. (2018) A Computer Program in MatLab for Obsidian Hydration Age Computations. *International Association for Obsidian Studies Bulletin* 59: 9-18.

Rogers, A. K., and D. Duke (2011) An Archaeologically Validated Protocol for Computing Obsidian Hydration Rates from Laboratory Data. *Journal of Archaeological Science* 38: 1340-1345.

Rogers, A. K., and D. Duke (2014a) Estimating Obsidian Hydration Rates from Time-Sensitive Artifacts: Method and Archaeological Examples. *International Association for Obsidian Studies Bulletin* 51: 31-38.

Rogers, A. K., and D. Duke (2014b) Unreliability of the Induced Hydration Method with Abbreviated Hot-Soak Protocols. *Journal of Archaeological Science* 52: 428-435.

Rogers, A. K., and D. Duke (2018) *Obsidian Hydration Dating at Bonneville Estates Rockshelter*, paper presented at the 2018 Great Basin Anthropological Conference, Salt Lake City, Utah.

Rogers, A. K. and R. M. Yohe II (2016) A Case Study in Site Formation Effects on Obsidian Hydration Dating. *International Association for Obsidian Studies Bulletin* 55: 5-9.

Rogers, A. K., and C. M. Stevenson (2014) Transient and Equilibrium Solubility of Water in Rhyolitic Glass: Implications for Hydration Rate Development at Elevated Temperature. *Journal of Archaeological Science* 45: 15-19.

Rogers, A. K., and C. M. Stevenson (2019) A Hydration Rate for Queen Obsidian, Western Nevada, Based on Density and Water Content. *International Association for Obsidian Studies Bulletin* 61: 24-28.

Schiffer, M. E. (1987) *Site Formation Processes of the Archaeological Record*. University of Utah Press, Salt Lake City.

Smith, G. M., P. Barker, E. Hattori, and T. Goebel (2013) Points in Time: Direct Radiocarbon Dates on Great Basin Projectile Points. *American Antiquity* 78(3): 580-594.

Steffen, A. (2005) *The Dome Fire Obsidian Study: Investigating the Interaction of Heat, Hydration, and Glass Geochemistry*. Unpublished PhD Dissertation, Department of Anthropology, University of New Mexico.

Stevenson, C. M., and B. E. Scheetz (1989) Induced Hydration Rate Development of Obsidians from the Coso Volcanic Field: A Comparison of Experimental Procedures. In *Current Directions in California Obsidian Studies,* edited by R. E. Hughes, pp. 23-30. Contributions of the University of California Archaeological Research Facility No. 48.

Stevenson, C. M., E. Knauss, J. J. Mazer, and J. K. Bates (1993) The Homogeneity of Water Content in Obsidian from the Coso Volcanic Field: Implications for Obsidian Hydration Dating. *Geoarchaeology* 8(5): 371-384.

Stevenson, C. M., J. J. Mazer, and B. E. Scheetz (1998) Laboratory Obsidian Hydration Rates: Theory, Method, and Application. In *Archaeological Obsidian Studies: Method and Theory. Advances in Archaeological and Museum Science*, Vol. 3, edited by M. S. Shackley, pp.181-204. Plenum Press, New York.

Stevenson, C. M., M. Gottesman, and M. Macko (2000) Redefining the Working Assumptions for Obsidian Hydration Dating. *Journal of California and Great Basin Anthropology* 22(2): 223-236.

Stevenson, C. M., I. M. Abdelrehim, and S. W. Novak (2004) High Precision Measurement of Obsidian Hydration Layers on Artifacts from the Hopewell Site Using Secondary Ion Mass Spectrometry. *American Antiquity* 69(4): 555-568.

Stevenson, C. M., and S. W. Novak (2011) Obsidian Hydration Dating by Infrared Spectroscopy: Method and Calibration. *Journal of Archaeological Science* 38: 1716-1726.

Stevenson, C. M., and A. K. Rogers (2014) Transient and Equilibrium Solubility of Water in Rhyolitic Glass: Implications for Hydration Rate Development at Elevated Temperature. *Journal of Archaeological Science* 45: 15-19.

Stevenson, C. M., A. K. Rogers, and M. D. Glascock (2019) Variability in Structural Water Content and its Importance in the Hydration Dating of Cultural Artifacts. *Journal of Archaeological Science: Reports* 23: 231-242.

Taylor, J. R. (1982) *An Introduction to Error Analysis.* University Science Books, Mill Valley, California.

Von Aulock, F. W., B. M. Kennedy, C. I. Schipper, J. M. Castro, D. E. Martin, C,. Oze, J. M. Watkins, P. J. Wallace, L. Puskar, F. Begue, A. R. L. Nichols, H. Tuffen (2014) Advances in Fourier Transform Infrared Spectroscopy of Natural Glasses: From Sample Preparation to Data Analysis. *Lithos* 206-207: 53-64.

West, G. J., W. Woolfenden, J. A. Wanket, and R. S. Anderson (2007) Late Pleistocene and Holocene Environments. In *California Prehistory: Colonization, Culture, and Complexity*, edited by T. L. Jones and K. A. Klar, pp. 11-34. Altamira Press, Walnut Creek, California.

Yohe, R. M., II (1992) *A Reevaluation of Western Great Basin Cultural Chronology and Evidence for the Timing of the Introduction of the Bow and Arrow to Eastern California based on new Excavations at the Rose Spring Site (CA-INY-372).* Unpublished PhD Dissertation, Department of Anthropology, University of California, Riverside.

Yohe, R. M., II (1998) The Introduction of the Bow and Arrow and Lithic Resource Use at Rose Spring (CA-INY-372). *Journal of California and Great Basin Anthropology* 20(1): 26-52.

Zhang, Y. (2008) *Geochemistry.* Princeton University Press, New Jersey.

Zhang, Y., E. M. Stolper, and G. J. Wasserburg (1991) Diffusion of Water in Rhyolytic Glasses. *Geochimica et Cosmochimica Acta* 55: 441-456.

Zhang, Y., R. Belcher, L. Wang, and Sally Newman (1997) New Calibration of Infrared Measurement of Dissolved Water in Rhyolitic Glasses. *Geochimica et Cosochimica Acta* 62: 3089-3100.

Zhang, Y, and H. Behrens (2000) H_2O Diffusion in Rhyolitic Melts and Glasses. *Chemical Geology* 169: 243-262.

APPENDIX A
AGE ANALYSIS CODE LISTING (MatLab)

```
% Program OHDCODEBL
% Update 12/16/2019
% Obsidian hydration analysis code baseline. Computes age in cyb2k, age
accuracy,
% and PE of the mean.
% Characteristics: Matrix I/O, lines 27 and 219.
% EHT by numerical integration for current conditions in SW Great Basin.
% Computes activation energy from inferred water content.
% Uses flow-specific hydration rates for Coso obsidian.
% Rates updated per SCA2013 paper.
% Rates for BH-E, BH-W, CDSR, CDLM, NGM, FS, and Queen added.
% Diurnal variation amplitude represented by cosine model.
%
%************************************************************************
%
% Module 1 - set constants
clear
% Uncertainty model for error sources
CVKE = 0.05; % CV of estimated hydration rate
YBZ = 0.5; % Default value of fraction of time artifact was at depth
SIGEHT = 1.0; % Std dev of EHT error, deg C
CVH = 0.06; %Rate std dev due to humidity
EHTR = 20.0; % Reference EHT for hydration rates, deg C
EHTRK = EHTR + 273.15; % Reference EHT for hydration rates, deg K
%
%************************************************************************
%
% Module 2 - Read input data from a .csv file
INDATA = csvread('C:\MATLAB701\work\CBFLIn.csv');
L = size(INDATA,1);
for jj = 1:L % j is index for sequence number.
   No  = INDATA(jj,1); %No =  Sequence Number
   alt = INDATA(jj,2); %alt = Altitude of archaeological site, ft
   rim = INDATA(jj,3); %rim = Uncorrected rim thickness, microns
   sig = INDATA(jj,4); %sig = Rim standard deviation, microns
   z   = INDATA(jj,5)/100; %z  = Burial depth of artifact, meters
   NS  = INDATA(jj,6); %NS =  Sample size
   FL  = INDATA(jj,7); %FL =  Obsidian source flow: SLM=1,WSL=2,WCP=3,JRR=4,BH
= 5,
   % CDSR = 6, CDLM = 7, Queen =8, NGM = 9, FS = 10, Obs Butte = 11, Saline
   % Range = 12, Mt Hicks = 13, Mono Glass Mtn = 14
   NOM = INDATA(jj,8); % Nominal condition flag; 1 = surface, 2 = mixed, 3 =
depth
%
%************************************************************************
%
% Module 3 - Compute obsidian parameters from hydration rate
%
% Parameters for aggregate Coso volcanic field
ratecal = 22.86; % Default rate for Coso volcanic field, u^2/1000 yrs @ 20 deg
C
CVKS = 0.33;
% Set parameters for individual flows
```

```
    if FL == 1 % SLM
        ratecal = 29.87;
        CVKS = .13;
    end
    if FL == 2 % WSL
        ratecal = 18.14;
        CVKS = .20;
    end
    if FL == 3 % WCP
        ratecal = 27.28;
        CVKS = .25;
    end
    if FL == 4 % JRR
        ratecal = 22.27;
        CVKS = .26;
    end
    if FL == 5 % Bodie Hills
        ratecal = 14.2;
        CVKS = .15;
    end
    if FL == 6 % Casa Diablo Sawmill Ridge
        ratecal = 12.37;
        CVKS = .15;
    end
    if FL == 7 % Casa Diablo Lookout Mtn
        ratecal = 12.05;
        CVKS = .15;
    end
    if FL == 8 % Queen
        ratecal = 10.29;
        CVKS = .15;
    end
    if FL == 9 % Napa Glass Mtn
        ratecal = 12.05;
        CVKS = .1;
     end
     if FL == 10 % Fish Springs
        ratecal = 11.26;
        CVKS = .15;
     end
        if FL == 11 % Obsidian BUtte
        ratecal = 9.27;
        CVKS = .15;
     end
     if FL == 12 % Saline Range
        ratecal = 9.96;
        CVKS = .15;
     end
     if FL == 13 % Mt. Hicks
        ratecal = 11.90;
        CVKS = .15;
     end
     if FL == 14 % Mono Glass Mountain
        ratecal = 9.97;
        CVKS = .15;
     end
ageconst = 1000/ratecal;
```

```
% Compute water concentration
water = (log(ratecal)-(37.76-10433/EHTRK))/(-2.289+1023/EHTRK);
% Compute E/R
EoverR = 10433-1023*water; % deg K
%
%**********************************************************************
%
% Module 4 - Temperature model
% Compute temperature parameters for site.
    STA   = 22.71 - 0.002*alt; % Annual Average temperature
    SVA   = 24.25 - 0.0006*alt; % Annual temperature variation, surface
    SVDM  = 18.49 - 0.0007*alt; % Mean diurnal variation, surface
    SVDAM = 2.08; % Amplitude of diurnal variation, surface.
%
%**********************************************************************
%
% Module 5 - Compute Keff and EHT
% Surface conditions
DIUP = 2*pi/24; %diurnal period in radians/hour
ANNP = 2*pi/(24*365); % annual period in radians/hour
Nyears = 1; % Length of integration period, years
MM = Nyears*365*24; % Number of data points to integrate
Kint = 0;
for I = 1:MM
   SVD = SVDM + SVDAM*cos(ANNP*I);
   k      =      exp(-EoverR/((STA+273.15)      +      (0.5*SVD*cos(DIUP*I))+
(0.5*SVA*cos(ANNP*I)))));
   Kint = Kint + k;
end
Keffsurf = Kint/MM;
EHTKS = -EoverR/(log(Keffsurf)); % EHT in deg K at surface
EHTCS = EHTKS - 273.15; % EHT at surface in deg C
% Compute Keff and EHT at artifact depth
SVAB = SVA*exp(-0.44*z); % Annual variation @ artifact recovery depth
Kint = 0;
for I = 1:MM
   SVDB = (SVDM + SVDAM*cos(ANNP*I))*exp(-8.5*z); % Diurnal variation @ artifact
recovery depth
   k      =      exp(-EoverR/((STA+273.15)      +      (0.5*SVDB*cos(DIUP*I))+
(0.5*SVAB*cos(ANNP*I)))));
   Kint = Kint + k;
end
Keff = Kint/MM;
EHTKD = -EoverR/(log(Keff)); % EHT at artifact depth, deg K
EHTCD = EHTKD-273.15; % EHT at artifact depth, deg C
% Compute effective K and EHT for artifact buried YB fraction of its life.
Keffaverage = (1-YBZ)*Keffsurf+YBZ*Keff;
EHTKA = -EoverR/log(Keffaverage); % Average EHT, deg K
%
%**********************************************************************
%
% Module 6 - Age computation
TEMPFACR = EoverR/EHTRK; % Temperature factor, reference conditions
% Surface conditions
TEMPFACS = EoverR/EHTKS; % Temperature factor
RCFS = exp((-TEMPFACR+TEMPFACS)/2); %Rim correction
rimprimeS = rim*RCFS; % Rim corrected to rate EHT
```

```
t1S = ageconst*rimprimeS^2; % Age
% Conditions at depth
TEMPFACD = EoverR/EHTKD; % Temperature factor
RCFD = exp((-TEMPFACR+TEMPFACD)/2); % Rim correction
rimprimeD = rim*RCFD; %Rim corrected to reference EHT
t1D = ageconst*rimprimeD^2; % Age
% Conditions for artifact buried YB fraction of time
TEMPFACA = EoverR/EHTKA; % Temperature factor
RCFA = exp((-TEMPFACR+TEMPFACA)/2); % Rim correction factor
rimprimeA = rim*RCFA; % Rim corrected to reference EHT
t1A = ageconst*rimprimeA^2; % Age
% EHT corrected rim SD
SDprime = sig*RCFA;
%
%********************************************************************
%
% Module 7 - Source/process model standard deviation
Labvar = 0;
EHTvar = 0;
Watervar = 0;
Ratevar = 0;
SFvar = 0;
Humvar = 0;
if rim > 0
   Labvar = 4*(sig/rim)^2; % Rate variance due to rim reading
   EHTvar = (0.12*SIGEHT)^2; % Rate variance due to EHT uncertainty
   Watervar = CVKS^2; % Rate variance due to intrinsic water variations
   Ratevar = CVKE^2; % Rate variance due to ascribed rate
   Humvar = CVH^2; %Rate variance due to humidity
   SFvar = ((t1S-t1D)^2)/12; % Age uncertainty variance due to site formation
processes
end
% Select which case to use as nominal - surface, mixed, or depth
% Default is mixed (NOM = 2)
t1N = t1A;
if NOM == 1
    t1N = t1S;
end
if NOM == 3
   t1N = t1D;
end
MODSD   =   sqrt((Labvar+EHTvar+Watervar+Ratevar+Humvar)*t1N^2+SFvar);   %
Source/process model standard deviation
%
%********************************************************************
%
% Module 8 - Output data as .csv file
OUTDATA(jj,1) = No; % sequence no.
OUTDATA(jj,2) = alt; % site altitude, ft
OUTDATA(jj,3) = STA; % Annual temp, deg C
OUTDATA(jj,4) = SVA; % Annual variation, deg C
OUTDATA(jj,5) = SVD; % Mean diurnal variation, deg C
OUTDATA(jj,6) = EHTCS;% EHT on surface
OUTDATA(jj,7) = rim; % uncorrected rim mean, microns
OUTDATA(jj,8) = sig; % Uncorrected rim sd, microns
OUTDATA(jj,9) = z; % artifact burial depth, m
OUTDATA(jj,10)= NS; % sample size
```

```
OUTDATA(jj,11)= FL; % Obsidian flow
OUTDATA(jj,12)= rimprimeA; %EHT corrected rim mean
OUTDATA(jj,13)= SDprime; % Rim SD, corrected for EHT
OUTDATA(jj,14)= t1S; % Age for surface conditions
OUTDATA(jj,15)= t1D; % Age at depth
OUTDATA(jj,16)= t1A; % Age for artifact buried YB fraction
OUTDATA(jj,17)= MODSD; % Source/process SD of age, yrs +/-
OUTDATA(jj,18)= MODSD/sqrt(NS) ; % Probable error of the mean
OUTDATA(jj,19)= t1N*sqrt(Labvar); % Age variance due to rim reading
OUTDATA(jj,20)= t1N*sqrt(EHTvar); % Age variance due to EHT uncertainty
OUTDATA(jj,21)= t1N*sqrt(Watervar); % Age variance due to intrinsic water
variations
OUTDATA(jj,22)= t1N*sqrt(Ratevar); % Age variance due to ascribed rate
OUTDATA(jj,23)= t1N*sqrt(Humvar); % Age variance due to humidity
OUTDATA(jj,24)= sqrt(SFvar); % Age variance due to site formation processes
OUTDATA(jj,25)= NOM; % Nominal condition flag value
OUTDATA(jj,26)= ratecal;
end
dlmwrite('CBFLOut.csv', OUTDATA, ',')
fprintf('Run Complete')
```

APPENDIX B
CODE FOR ASSIGNING TEMPORAL BINS (MatLab)

```
% Program TemporalBins
% Assigns OHD dates to temporal bins based on mean and std. dev.
clear
% Set temporal bin boundaries
    L(1) = 0;      %Present
    L(2) = 150;    %Historic period start
    L(3) = 900;    %Marana period start
    L(4) = 1800;   %Haiwee period start
    L(5) = 4000;   %Newberry period start
    L(6) = 8000;   %Pinto period start
    L(7) = 10000;  %Lake Mohave period start
    L(8) = 14000;  %Paleoindian period start
    L(9) = 23000;  %LGM, PHT start
    L(10)= 50000;
% Clear temporal bins
for k = 1:9
    ABS(k) = 0;
end
%
%************************************************************************
% Read input data
INDATA = csvread('C:\MATLAB701\work\InputData.csv');
LL = size(INDATA,1);
for jj = 1:LL % jj is index for sequence number.
   SN  = INDATA(jj,1); %Sequence Number
   age = INDATA(jj,2); %Mean age, cal BP
   sda = INDATA(jj,3); %Std. Dev of age, yrs
%
%************************************************************************
% Compute date probabilities for each bin
    for k = 1:9
        t(k) =   (age-L(k))/(2*sda);
        A = abs(erf(t(k)));
        t(k+1) = (age-L(k+1))/(2*sda);
        B = abs(erf(t(k+1)));
        if ((age >= L(k)) & (age <= L(k+1)));
            AB(k)= (A + B)/2;
        else
            AB(k) = abs(A - B)/2;
        end
        ABS(k) = ABS(k)+AB(k);
    end
end
% Create index numbers (first column of output matrix)
for k = 1:9
    OUTDATA(k,1) = k;
end
% Create second column of output matrix
for k = 1:9
    OUTDATA(k,2) = ABS(k);
end
% Output data file
dlmwrite('OutputData.csv', OUTDATA, ',')
```

```
fprintf('Run Complete\n')
% Print data
fprintf('\n')
fprintf('Date distribution\n')
fprintf('Historic period........................%6.2f\n' ,ABS(1))
fprintf('Marana Period..........................%6.2f\n', ABS(2))
fprintf('Haiwee Period..........................%6.2f\n', ABS(3))
fprintf('Newberry Period........................%6.2f\n', ABS(4))
fprintf('Pinto Period...........................%6.2f\n', ABS(5))
fprintf('Lake Mohave Period.....................%6.2f\n', ABS(6))
fprintf('Paleoindian Period.....................%6.2f\n', ABS(7))
fprintf('Pleistocene-Holocene Transition.......%6.2f\n', ABS(8))
fprintf('Prior..................................%6.2f\n', ABS(9))
fprintf('\n')
```

APPENDIX C
Excel Workbook for OHD Analysis.

	A	B	C	D	E	F	G	H	I	J	K	L	M	N	O	P	Q	R	S	T
1	Spec. No.	Rm, u	SDm, u	z, cm	Source	Rate	Rate CV	Rate EHT, deg C	Ta, deg C	Va0, deg C	Vd0, deg C	Va, deg C	Vd, deg C	EHT, deg C	RCF	Rc, u	SDc, u	Age CV	Age, cyb2k	Age SD, yrs
2	1	8.00	0.08	10.00	WSL	18.14	0.15	20.00	15.00	21.00	18.00	20.10	7.69	17.87	1.13	9.06	0.09	0.29	4528	1305
3																				
4																				
5																				
6																				
7																				
8																				
9																				
10																				
11																				
12																				
13																				
14																				
15																				
16																				
17																				
18																				
19																				
20																				
21																				
22																				
23																				
24																				
25																				
26																				
27																				
28																				
29																				
30																				
31																				

ABOUT OUR WEB SITE

The IAOS maintains a website at http://www.deschutesmeridian.com/IAOS/ The site has some great resources available to the public, and our webmaster, Craig Skinner, continues to update the list of publications and must-have volumes.

You can now become a member online or renew your current IAOS membership using PayPal. Please take advantage of this opportunity to continue your support of the IAOS.

Other items on our website include:

- World obsidian source catalog
- Back issues of the *Bulletin.*
- An obsidian bibliography
- An obsidian laboratory directory
- Photos and maps of some source locations
- Links

Thanks to Craig Skinner for maintaining the website. Please check it out!

CALL FOR ARTICLES

Submissions of articles, short reports, abstracts, or announcements for inclusion in the *Bulletin* are always welcome. We accept submissions in MS Word. Tables should be submitted as Excel files and images as .jpg files. Please use the *American Antiquity* style guide for formatting references and bibliographies. http://www.saa.org/Portals/0/SAA%20Style%20Guide_Updated%20July%202018.pdf

Submissions can also be emailed to the *Bulletin* at IAOS.Editor@gmail.com Please include the phrase "IAOS Bulletin" in the subject line. An acknowledgement email will be sent in reply, so if you do not hear from us, please email again and inquire.

Deadline for Issue #64 is May 1, 2020.

Email or mail submissions to:

Dr. Carolyn Dillian
IAOS Bulletin, Editor
Department of Anthropology & Geography
Coastal Carolina University
P.O. Box 261954
Conway, SC 29528
U.S.A.

Inquiries, suggestions, and comments about the *Bulletin* can be sent to IAOS.Editor@gmail.com Please send updated address information to Matt Boulanger at Boulanger.Matthew@gmail.com

MEMBERSHIP

The IAOS needs membership to ensure success of the organization. To be included as a member and receive all of the benefits thereof, you may apply for membership in one of the following categories:

Regular Member: $20/year*
Student Member: $10/year or FREE with submission of a paper to the *Bulletin* for publication. Please provide copy of current student identification.
Lifetime Member: $200

Regular Members are individuals or institutions who are interested in obsidian studies, and who wish to support the goals of the IAOS. Regular members will receive any general mailings; announcements of meetings, conferences, and symposia; the *Bulletin*; and papers distributed by the IAOS during the year. Regular members are entitled to vote for officers.

*Membership fees may be reduced and/or waived in cases of financial hardship or difficulty in paying in foreign currency. Please complete the form and return it to the Secretary-Treasurer with a short explanation regarding lack of payment.

NOTE: Because membership fees are very low, the IAOS asks that all payments be made in U.S. Dollars, in international money orders, or checks payable on a bank with a U.S. branch. Otherwise, please use PayPal on our website to pay with a credit card.
http://www.deschutesmeridian.com/IAOS/membership.html

For more information about membership in the IAOS, contact our Secretary-Treasurer:

Matthew Boulanger
Department of Anthropology
Southern Methodist University
P.O. Box 750336
Dallas, TX 75275-0336
U.S.A.
Boulanger.Matthew@gmail.com

Membership inquiries, address changes, or payment questions can also be emailed to Boulanger.Matthew@gmail.com

---

ABOUT THE IAOS

The International Association for Obsidian Studies (IAOS) was formed in 1989 to provide a forum for obsidian researchers throughout the world. Major interest areas include: obsidian hydration dating, obsidian and materials characterization ("sourcing"), geoarchaeological obsidian studies, obsidian and lithic technology, and the prehistoric procurement and utilization of obsidian. In addition to disseminating information about advances in obsidian research to archaeologists and other interested parties, the IAOS was also established to:

1. Develop standards for analytic procedures and ensure inter-laboratory comparability.
2. Develop standards for recording and reporting obsidian hydration and characterization results
3. Provide technical support in the form of training and workshops for those wanting to develop their expertise in the field.
4. Provide a central source of information regarding the advances in obsidian studies and the analytic capabilities of various laboratories and institutions

MEMBERSHIP RENEWAL FORM

We hope you will continue your membership. Please complete the renewal form below.

NOTE: You can now renew your IAOS membership online! Please go to the IAOS website at http://www.deschutesmeridian.com/IAOS/ and check it out! Please note that due to changes in the membership calendar, your renewal will be for the next calendar year. Unless you specify, the *Bulletin* will be sent to you as a link to a .pdf available on the IAOS website.

___ Yes, I'd like to renew my membership. A check or money order for the annual membership fee is enclosed (see below).

___ Yes, I'd like to become a new member of the IAOS. A check or money order for the annual membership fee is enclosed (see below). Please send my first issue of the IAOS *Bulletin*.

___ Yes, I'd like to become a student member of the IAOS. I have enclosed either an obsidian-related article for publication in the IAOS *Bulletin* or an abstract of such an article published elsewhere. I have also enclosed a copy of my current student ID. Please send my first issue of the IAOS *Bulletin.*

NAME: _____

TITLE: _____ AFFILIATION:_____

STREET ADDRESS: _____

CITY, STATE, ZIP: _____

COUNTRY: _____

WORK PHONE: _____ FAX: _____

HOME PHONE (OPTIONAL): _____

EMAIL ADDRESS: _____

My check or money order is enclosed for the following amount (please check one):
___ $20 Regular
___ $10 Student (include copy of student ID)
___ FREE Student (include copy of article for the *IAOS Bulletin* and student ID)
___ $200 Lifetime

Please return this form with payment:
(or pay online with PayPal http://www.deschutesmeridian.com/IAOS/paypal.html**)**

Matthew Boulanger
Department of Anthropology
Southern Methodist University
P.O. Box 750336
Dallas, TX 75275-0336
U.S.A.